Photovoltaic Solar Cell Technologies: *Bounds and Challenges*

Pabitra.K. Nayak[1]*, Suhas Mahesh[1], Henry J. Snaith[1], David Cahen[2]

[1]Clarendon Laboratory, University of Oxford, Parks Road, Oxford, OX1 3PU, UK

[2]Dept. of Materials & Interfaces, Weizmann Institute of Science, Rehovot, Israel, 76100.

* author for correspondence, email: pabitra.nayak@physics.ox.ac.uk

Abstract:

The remarkable development in photovoltaic (PV) technologies, including materials, cells and modules, over the past five years call for renewed assessments with an eye towards their future progress. We do not restrict such assessments to solar to electrical power conversion efficiencies (PCEs), but also consider many of the factors that affect power output for each cell type. Where appropriate, we note improvements in control over materials and interfaces, and discovery of new properties in materials. The PCE of "champion cells" for all types of PV technology has improved over the past half decade. We analyse and discuss the remarkable progress in cells and modules, based on single crystal -Si, GaInP and InP, and on thin (polycrystalline) films of , esp. CdTe and Cu(In,Ga)Se_2 (=CIGS). In addition, we analyse PV developments of the more recently emerged lead halide perovskites, together with notable improvements in sustainable chalcogenides, organics and quantum dots. By comparing PV cell parameters across technologies, we can appraise how far each technology may progress in the near future, because, even though accurate or revolutionary developments cannot be predicted, often cross-fertilization occurs, making achievements in one cell type an indicator of evolutionary developments in others. This is extremely relevant in the present time, since the common theme of metal halide perovskites has helped to unite previously disparate, technology-focussed strands of PV research.

Introduction:

Undoubtedly, sunlight is the most abundant, safe and clean energy source for sustainable economic growth. One of the efficient and practical ways to use the sunlight as an energy source is to convert it to electricity using solar cells. An upper limit for light to electrical power conversion efficiency, PCE, by a single junction solar cell (i.e., solar photon energy → electrical energy) is given by the Shockley-Queisser (S-Q) model and formalism[1]. In this formalism there are assumptions, which postulate that all photons with energies above the bandgap create free electrons and holes, with perfectly charge-selective contacts, thus yielding one electron per absorbed photon to the electrical current flow. The S-Q model also stipulates that all electron-hole recombination events, which occur when the solar cell is generating power, are the inverse process to light absorption and therefore radiative – i.e., they re-sult in the re-emission of light. The S-Q limit is based purely on thermodynamic considerations and takes the optical absorption edge (E_G), the solar spectrum and the operating temperature of the solar cell as the only inputs for the PCE calculation. The efficiency of real-world single junction solar cells will always be below the S-Q limit as real material properties come into play, e.g., the absorption edge is not a step function, as assumed by the S-Q model, and real materials have defects, which will lead to non-radiative recombination, i.e. the generation of heat, instead of re-emission as light. However, realistic goals can be set, based on present-day performance and on understanding the fundamental limits associated with a particular cell type and technology, to assess how the real-world cells deviate from their S-Q limit, and how they can be adapted to more closely approach this limit.

In our previous work, [2,3] we used the optical bandgap values of the absorbing material, wherever a reliable value was available, and in other cases the onset of the external quantum efficiency (EQE), which can be subjective, to compare the solar cell parameters. In this work, we adopt the 'distributed S-Q gap method'[4] to define the bandgap, allowing a consistent comparison between technologies. We update the experimental values which have changed due to the all-around developments in all the types of solar cell technologies. We *discuss reasons behind* the recent (past 5 years) developments in solar cell performance parameters and in how far they can be expected to improve further with the available technology and the current state-of-the-art materials quality. We also focus on the interfaces and their impact on solar cell performance and discuss how the evolution of interfacial materials con-tributed towards the development of solar cells.

We present the rationale behind the theoretical assessment of solar cell efficiencies, highlighting and quantifying the parallel impacts of both electronic disorder in the solar absorber material, and of elec-tron-hole recombination (radiative vs. non-radiative). We derive a simple analytical relation between the open-circuit voltage, V_{OC}, and a few properties of the solar absorber material and the solar cells, making it possible to accurately estimate the V_{OC} or radiative efficiency of a cell, requiring only basic

mathematical skills. One of our key inference is that the PCE loss, due to electronic disorder and of sizeable binding energy of excitons, has been almost completely eliminated in the latest organic solar cells. The main remaining parameter required to make cells based on the conjugated organic semiconductors competitive with the best technologies, is to enhance their radiative efficiency. On the downside we assess that contemporary "sustainable" chalcogenide thin-film materials have such a high level of intrinsic static disorder that they will be incapable of yielding competitively efficient solar cells and, barring drastic developments to bypass the disorder issue, are likely to follow the fate of amorphous Si-based cells, which also have too high a degree of static electronic disorder to deliver a competitively efficient PV cell.

Arguably, the most remarkable progress over the last half decade has been with halide perovskite-based devices, where PCE of laboratory cells now match those of the best established inorganic (poly-/multi-) crystalline technologies. While published large area cell, and especially module performances, as well as cell stabilities, still lag behind those of established PV technologies, the rate of improvement in large area cell performance and cell stability is quite promising. Taking cues from development of other PV technologies, we can extrapolate that these cells will soon match those of the more mature polycrystalline technologies. Where possible our discussions include an assessment of factors, responsible for the improvements for each cell type.

Defining the photovoltaic bandgap:

How well a semiconductor is suited as solar absorber material in a PV cell, is primarily governed by its band gap value, E_G. However, despite this being a fundamental material property, there remains considerable ambiguity over how to determine E_G, and which methods for determining E_G are most relevant for PV. Often reliable optical bandgap values are not available. Without reliable optical absorption data to extract bandgaps we cannot make objective comparisons of cell parameters, V_{OC}, V_{MP}, J_{SC}, J_{MP} and FF (see FIG. S1 for definitions) of different cell types. With the increasing prominence of new types of cells, particularly the metal halide perovskites (ABX_3), sustainable chalcogenides, like $Cu_2ZnSnS_{4-y}Se_y$(CZTSS), Cu_2ZnSnS_4 (CZTS), and organic photovoltaics (OPV), which often lack reliable bandgap values, or indeed a definition of a band gap with the latter, here we use the External Quantum Efficiency (EQE) data to determine a "photovoltaic gap", E_g^{PV}, which is, following Rau et al.[4], a weighted distribution of S-Q band gaps (See FIG. S2 and Table S1 for the comparison with known optical bandgaps, or lowest optical transition energies)

E_g^{PV} is given by:

$$E_g^{PV} = \int_a^b E_g P(E_g)\, dE_g / \int_a^b P(E_g)\, dE_g \,, \qquad (1)$$

where $P(E_g) = \frac{d}{dE} EQE(E)$ is the probability distribution function of the distribution of SQ-type band-gap energies.

Hence, the maximum of $(\frac{d}{dE} EQE)$ gives an approximate E_g^{PV} value, and can be used for all practical purposes, if $P(E_g)$ is approximately Gaussian. To avoid noisy data, the integration limits are set to *a* and *b*, the photon energies for which $P(E_g)$ equals 50% of its maximum on either side of that maximum.

E_g^{PV} is called the PV gap, to stress that its value need not be and often will not be the same as that, determined from pure optical experiments, the optical band gap. As a simple illustration, if a solar absorber material is made increasingly thicker, E_g^{PV} of a cell composed of this absorber will shift to lower and lower energy. However, the optical band gap, a property of the material, will be unchanged.

Gao and co-workers[5] analysed some different ways to determine the relevant bandgap for solar cells. For OPVs, they suggest that the intersection point of absorption and emission spectra of the lowest bandgap material can be used as an effective optical bandgap. However, E_g^{PV}, determined by a physically meaningful extension of the SQ theory and mathematically consistent way, is to compare the solar cell parameters between different types and architectures of PV cells[4].

Energy losses:

Due to thermodynamic factors (eqn. 2, below), at temperatures > 0 Kelvin it is not possible to convert all the energy associated with the separated electron-hole pair into usable free energy, even after thermalization of the carriers to the band edges. The V_{OC} of a solar cell in the SQ limit is given by equation 2 [6,7] (In the SI we show the derivation of the analytical expression of qV_{OC}^{SQ}).

$$qV_{OC}^{SQ} = E_g^{PV}\left(1 - \frac{T_A}{T_S}\right) + kT_A \ln\left(\frac{\gamma(E_g^{PV}, T_S)}{\gamma(E_g^{PV}, T_A)}\right) - kT_A \ln\left(\frac{\Omega_{out}}{\Omega_{in}}\right) \qquad (2)$$

where $\gamma\left(E_g^{PV}, T\right) = T(E_g^{PV\,2} + 2kTE_g^{PV} + 2k^2T^2)$

Here we use E_g^{PV}, the PV gap, as equivalent to the S-Q bandgap of the absorber in the solar cell, q is the elementary charge, T_A, T_S are the temperatures (in Kelvin) of the solar cell and the sun, respectively, Ω_{out} and Ω_{in} represent the solid angles for the emitted and absorbed photons, respectively, k is the Boltzmann constant.

Attaining the radiative limit - the situation where at open circuit the photogenerated carriers can escape the system only as emitted photons - does not require a step-function absorptance. Correspondingly, the V_{OC} of the cell in the radiative limit, V_{OC}^{Rad}, can be different from V_{OC}^{SQ}, due to the cell's

absorptance not being a step function. Through considerations, which we highlight in the SI (APPENDIX 1), the less steep the rise in EQE, the larger the dark recombination current density, and the lower V_{OC}^{Rad} is with respect to V_{OC}^{SQ}. We will refer to this loss as the "radiative recombination loss".

Due to the presence of non-radiative recombination in any real PV system, and sub-unity efficiency of photon out-coupling, the experimentally achieved V_{OC} values of solar cells are lower than the radiative limit (V_{OC}^{Rad}) and are given by[8,9]

$$qV_{OC}^{cell} = qV_{OC}^{Rad} - kT_A|\ln(\eta_{ext})| \quad (3)$$

where η_{ext} is the external quantum efficiency for electroluminescence (EQE_{EL}) of the solar cell.

At open circuit (OC) the net rate of flow of the charge carriers from the cell is zero (→ zero power output) and, because of that, the difference in the electrochemical potentials for the electrons and holes remains highest. Between OC and short circuit (SC) there is a voltage (V_{MP})-current (I_{MP}) combination that yields the maximum power (MP); then the non-zero rate of flow of charge carriers from the cell lowers the steady state concentrations of the carriers inside the cell and, thus, affects their chemical potentials, so that V_{MP} is related to V_{OC} and always $< V_{OC}$. (See '*relation between* V_{MP} *and* V_{OC}' section in the SI). The operational loss (OL) in energy in a solar cell is thus given by $E_g^{PV} - qV_{MP}$. All the loss mechanisms that contribute to the total OL can be listed as follows.

$$OL = SQ\ loss + Radiative\ recombination\ loss\ beyond\ SQ\ limit + Nonradiative\ recombination\ loss + Loss\ due\ to\ operation\ at\ MP \quad (4)$$

Mathematically, the OL can be expressed as (See the section *'Operational Loss'* in the SI)

$$OL = \left(E_g^{PV}\frac{T_A}{T_S}\right) - kT_A\ln\left(\frac{\gamma\left(E_g^{PV},T_S\right)}{\gamma\left(E_g^{PV},T_A\right)}\right) + kT_A\ln\left(\frac{\Omega_{out}}{\Omega_{in}}\right) + kT_A\ln\left(\frac{J_{SC}^{SQ}}{J_{SC}}\right) + kT_A\ln\left(\frac{J_0^{Rad}}{J_0^{SQ}}\right) + kT_A\ln|(P_{esc})| + kT_A\ln\left|\left(\frac{\eta_{int}}{1-\eta_{int}\cdot P_{reabs}}\right)\right| + nkT_A\ln\left(\frac{qV_{OC}^{cell}}{nkT_A} - \ln\left(\frac{qV_{OC}^{cell}}{nkT_A}+1\right)+1\right) \quad (5)$$

Here J_{SC}^{SQ} and J_0^{SQ} are the short circuit photo-current density and dark saturation current density in the S-Q limit, and J_0^{Rad} is the dark saturation current density in the radiative limit. η_{int} is the internal luminescence efficiency, P_{esc} or P_{reabs} are the probabilities that a photon escapes or is re-absorbed by the cell, respectively. In FIG. 1 (a) we illustrate the components contributing to the operational loss. In the right hand side of equation 5, the first three terms correspond to the loss at OC in the S-Q limit which is unavoidable in any single junction cell. The loss shows a quasi-linear relationship with E_g^{PV} (see FIG. S4), for E_g^{PV} between 2.5 to 1 eV, which spans almost all band gaps of interest for solar

cells. This allows us to provide the following vastly simplified analytical expression to calculate the V_{OC}^{SQ} of a cell operating at room temperature (298 K).

$$qV_{OC}^{SQ} = 0.941E_g^{PV} - 0.171\ eV \qquad (6)$$

The slope of the qV_{OC}^{SQ} versus E_g^{PV} is dominated by the first term of equation 2, and the value $\left(1-\frac{T_A}{T_S}\right)$ at 298K is 0.95. Since the other E_g^{PV}-dependent terms are in the arguments of logarithms in the second term of Equation 2, they only contribute marginally to the slope, resulting in a slight reduction in the slope. The intercept of the qV_{OC}^{SQ} vs. E_g^{PV} plot is mainly determined by the E_g^{PV}-independent part of the 2nd term and the 3rd term of equation 2.

In FIG. 1b we plot qV_{OC}^{SQ} versus E_g^{PV} and also show the V_{OC} of the certified champion cells (see also table 1 and table S2 for solar cell efficiency, area and Fill factor). The 4th and the 5th term in the RHS of eqn. 5 correspond to the extra radiative recombination loss due to the non-step function absorptance in the cell, which depends mainly on the static electronic disorder in the absorber. Later we will return to discussing electronic disorder, which can be quantified by the steepness of the absorption onset, with the exponential gradient of the absorption tail termed the Urbach energy, E_U. High quality semiconductor materials typically have E_U of 7-15 meV, which results in an extra ~10 meV loss in V_{OC} in the radiative limit. The 6th and 7th term together ($kT_A|\ln(\eta_{ext})|$) correspond to the loss due the non-radiative recombination and inefficiency in photon out-coupling. These two terms depend on the electronic quality of absorber and interface material and on the device architecture. In FIG. 1b we show the expected qV_{OC} for different η_{ext} values, where $qV_{OC}^{SQ} = qV_{OC}^{Rad}$

We can modify eqn. 6 (at 298K) to be an accurate predictor of V_{OC} as function of E_g^{PV} and η_{ext} for a solar cell with relatively steep absorption onset, as

$$qV_{OC} = 0.941E_g^{PV} - (0.181 + 0.0257\ln(\eta_{ext}))\ eV \qquad (7)$$

The above analytical expression can be used to gauge the η_{ext} of a cell from its open circuit voltage and PV gap. To check usefulness of equation 7, we compared the η_{ext}, calculated from qV_{OC} and E_g^{PV} with the experimentally determined external electroluminescence efficiency for different types of GaInP and metal halide perovskite cells, c-Si and CIGS cells (See SI, FIG. S5 and Table S3) and we find a good match between the calculated and measured η_{ext}.

The 8th term in equation 5 represent the loss due to the operation at the MP. In FIG. 1 (c) we show the experimental operational loss in comparison to the loss in the S-Q model, $\left(E_g^{PV} - qV_{MP}^{SQ}\right)$, which is unavoidable for systems that fit the S-Q model. In real cells, there is also an additional loss due to the non-zero series resistance (R_S) of the charge collecting contacts. The difference between $\left(V_{OC}^{cell} - V_{MP}\right)$ and $(nkT_A/q)\ln\left(\frac{qV_{OC}^{cell}}{nkT_A} - \ln(\frac{qV_{OC}^{cell}}{nkT_A}+1)+1\right)$, gives this practical loss (Table 1, se-

cond column from right,), which is mainly dominated by the contacts that are an integral part of a solar cell. In FIG. 1d we plot the expected voltage loss versus the V_{OC} of a cell and the experimentally observed voltage loss.

The comparison, which we show in Figure 1d, illustrates that the energy loss, beyond V_{OC}, varies greatly among the different cell technologies. Thus, even though cells based on CIGS, CZTS and c-Si have similar V_{OC}, their loss beyond V_{OC} is different. The same holds for the group of c-InP, polycrystalline-$CdTe_{1-x}Se_{1-x}$ and a-Si, and for the ABX_3 and c-GaAs cells.

Photo-current Efficiency:

The maximum photocurrent density in the S-Q limit is represented by the green curve in FIG. S6a. The experimental photocurrents at short circuit and at maximum power for various cell types are added in the figure to provide a quick visual summary of current efficiencies. In Table 2 we show the data for J_{SC}/J_{SC}^{SQ}, which reflects the efficiency of photon capture, subsequent photocarrier generation and collection at the cell's contacts. For cell operation at the maximum power, J_{MP}/J_{SC} is determined by the open circuit voltage and we provide the following equation which represents the relation between J_{MP}, J_{SC} and V_{OC} (See the section *'Relation between J_{MP}/J_{SC} and V_{OC}'* in the SI for the derivation)

$$\frac{J_{MP}}{J_{SC}} = \frac{V'_{OC} - \ln(V'_{OC}+1)}{V'_{OC} - \ln(V'_{OC}+1) + 1} \qquad (8),$$

where $V'_{OC} = \frac{qV_{OC}^{cell}}{nkT_A}$

In FIG. S6b we plot the expected $\frac{J_{MP}}{J_{SC}}$ values from theory for two different values of the diode ideality factor and the experimentally determined $\frac{J_{MP}}{J_{SC}}$ values (also given in Table 2) vs. V_{OC}. The deviation from the ideal values (i.e. for n=1) indicates loss of photo-generated carriers, which otherwise could have improved cell efficiencies. The excess loss of photo-generated carriers beyond what is required to maintain the V_{MP} of the cell indicates the presence of more than one carrier recombination path in the system. The non-radiative carrier recombination, both in the bulk and at the interfaces, and the presence of shunt resistances, all contribute to the loss in photo-generated carriers. Not surprisingly we find that the single crystal-based device technologies, c-Si, c-InP, c-GaAs, c-GaInP show the highest $\frac{J_{MP}}{J_{SC}}$ values, whereas those based on two polycrystalline materials, CZTSS, CZTS and on

amorphous Si, show the poorest $\frac{J_{MP}}{J_{SC}}$ values. In the next sections, we discuss the observed photocurrent efficiencies along with the progress, performance and losses, associated with each PV technology.

PROGRESS AND PERFORMANCE OF SOLAR CELLS

SINGLE CRYSTALLINE CELLS

c- GaAs: A single crystalline GaAs-based solar cell has shown the highest PCE (29.1%) of any single-junction cell. A remarkable improvement in V_{OC} was achieved when the cells were based on monocrystalline thin films, made by epitaxial lift-off, which allowed use of highly reflecting back contacts instead of substrates that introduce parasitic absorbance . The near unity photoluminescence quantum yield (PLQY) of the absorber material (~ 99.7 %[10]), suppression of non-radiative recombination at the charge collecting interfaces and the highly reflecting back contact help the photons to be recycled (See FIG. 2a,b and c) before they escape the cell from the front surface. All these factors translated into a near-unity value of η_{ext} or external radiative efficiency[11] of the cell. Since GaAs has a very sharp absorption onset, ($\rightarrow J_0^{SQ} \approx J_0^{Rad}$), with η_{ext} approaching unity, the V_{OC} closely approaches the S-Q limit[12] (FIG 1b). We notice that the $\frac{J_{MP}}{J_{SC}}$ value is also close to optimal for the cell's V_{OC}, indicating that only the fundamental loss in photo-current to operate at the V_{MP} happens in this cell and other factors have been supressed. The remaining loss in photo-current could be due partly to shadowing from the top contact of the cell, which can be avoided if an all-back contact configuration can be realized.

c- GaInP: Like GaAs, progress in GaInP technology has been mostly due to development of cell architectures [13]. Use of an absorbing GaAs substrate in an upright configuration (FIG. S7a) for GaInP, likely $Ga_{0.5}In_{0.5}P$ (P_{esc} = 0.015; P_{reabs} = 0.60) can yield η_{ext} = 0.04, for $\eta_{int} = 1$, while inverted GaInP solar cells (FIG. S7a) with a good Au back reflector (P_{esc} = 0.024; P_{reabs} = 0.90) can reach η_{ext} = 0.25. The change in device architecture to the inverted structure with Au back reflector pushed cell efficiency to 20.8%, by improving V_{MP} and $V_{OC,}$[13]. Further improvement in the PCE to 21.4% came from using slightly higher bandgap GaInP [14,13,15] (FIG. S8b), which improved the voltage of the cell further. The photo-current efficiency improved due to better collection of carriers generated from the higher energy photons, presumably due to the improved electronic quality of GaInP. The high $\frac{J_{MP}}{J_{SC}}$ and low OL for a 0.25 cm^2 cell show that this technology is getting closer to the efficiencies (relative to the bandgap), obtained with GaAs.

c-InP: The champion cell based on crystalline InP has now an efficiency of 24.2%, a significant improvement from the previous 22.1%. In the new cell, both J_{SC} and V_{OC} of the cell were improved. The improvement in photo-current efficiency is due to the high-low (HL) doping scheme employed in the

emitter layer(See SI), whereas the improvement in the V_{OC} is due to the (Al,In)As back-surface confinement layer (BSCL) (See FIG. 2 d) [16]. The operational loss as well as the photo-current efficiency (see FIG. 1c and S6a) in this technology are still far from their theoretical limits. With a PV gap and material properties similar to GaAs and GaInP, we can expect the efficiency of this technology to edge closer to that of GaAs in the coming years, provided the interfacial recombination and parasitic absorbance can be taken care of.

c-Si: For almost 18 years the best efficiency of the c-Si solar cell stood at 25% ; that 4 cm^2 c-Si solar cell was based on the so-called passivated emitter rear-localised (PERL) solar cell technology (FIG. 3a). It was clear, though, that there were losses from shadowing from the front grid and non-radiative surface recombination due to the contacts. The interdigitated back contacts (IBC) architecture (FIG. 3b) has the following advantages over the two-side contacted PERL cell:

(i) without a top grid, light trapping and passivation on the top surface can be expanded without shadowing effect, and

(ii) the electrodes at the back can be placed close to each other to lower the series resistance, which will decrease the OL.

To minimize non-radiative recombination at the surfaces due to the contacts, Si heterojunction (SHJ) technology (FIG. 3 c) has been adopted, where a thin film of intrinsic hydrogenated amorphous Si (i:a-Si) is introduced between the absorber, c-Si, and either an n- or p-doped a-Si layer, to decouple passivation from charge collection.

The champion c-Si cell, which has now a PCE of 26.7% (area = 79 cm^2), is an amalgam of concepts from silicon heterojunction (SHJ) and interdigitated back contacts (ICB) cells (FIG. 3d). Advances in processing technologies and continuing material development for the microelectronics industry to obtain high-grade electronic quality Si crystals made it possible to realise the present champion c-Si cell.

The question now arises if the new technological advancement can boost the efficiency of c-Si technology further. In our opinion, there is still room for improvements, particularly in the current efficiency. The photocurrent efficiency is less than the S-Q limit ($J_{sc}/J_{sc}^{SQ} = 96\%$, c.f. table 2) and comparable to that of the PERL cell, despite having no front electrodes.. The unavoidable loss in photo-current (1-2 %) is due to the filtering effect from the a-Si layer that is essential for the creation of the heterojunction. This loss manifests itself as a drop in EQE below 500 nm[17,18] (See figure S8) .The gaps between the rear electrodes are another cause for the photo-current loss, because light can pass through them, rather than be reflected back into the Si. This can be mitigated by using reflecting dielectric materials in the gaps. In sandwich-structured SHJ cells (FIG. 3c), where the p- and n-contacts are on either side of the wafer, V_{OC} of 750 mV has already been demonstrated;[19] hence we can expect ~10 mV [20] further V_{OC} improvement with the present SHJ-IBC architecture (cf. Table 1).

. The experimentally determined internal photoluminescence (PL) efficiency reported for the highest quality flat zone c-Si material with passivated surface is ~20% [21]. The commercially produced Si wafers have an order of magnitude lower internal PL efficiency [21] . This relatively low PL efficiency is due to the indirect bandgap of Si, which is an intrinsic material property that cannot be altered for this form of Si; the indirect character implies lower absorbance coefficient, meaning that more material is needed to absorb all the sunlight. This increase in volume of the material, compared to other PV absorber materials, and the long carrier lifetimes results in a situation where even small defect densities can cause significant non-radiative recombination.

POLY-(Multi-) CRYSTALLINE CELLS:

Multi-crystalline (mc-) Si: Unlike c-Si, mc-Si has inherent grain boundaries (GBs) and dislocations, which result in a poorer V_{OC} and V_{MP} than those of c-Si cells (c.f. Table1). Improvement in mc-Si technology in recent years is due to development of 'high-performance mc-Si (HP mc)', which has reduced structural defects[22]. Use of n-type HP mc-Si wafers takes the advantage of the higher minority carrier lifetime in n-type (holes) than in p-type (electrons) Si, due to the fact that Fe, one of the most important residual impurities in Si, is an effective *electron* scattering agent. [23] Use of such mc-Si allowed further performance improvement of m-Si–based cells[24]. The champion mc-Si cell uses a diffused boron front emitter and full-area tunneling oxide passivating rear contacts (TOPCon). The photo-current efficiency is comparable to that of c-Si cells and superior to that of the other polycrystalline material-based technologies. As expected, the operational loss is higher than of single crystal-based technologies.

CIGS:. When we compare the EQE of champion CIGS cells from the last few years, we find a noticeable difference (FIG. 4a) as cell performance improves. The EQE of the 19.8% efficient cell shows a drop below 520 nm. This is due to the combined effect of the inadequate diffusion length of the carriers and filtering from the CdS layer that is often used in these polycrystalline solar cells (See FIG. S9(a) for the schematic layout of CIGS cell) . CdS, which now is often replaced by ZnS, is needed for surface, and then interface, passivation, which increases V_{OC} but at the price of J_{SC}.

A major improvement in CIGS technology was a change in alkali metal ion treatment (from Na to K) after deposition of the CIGS layer. K^+ treatment modifies the chemical composition near the surface of the CIGS film by depleting Cu and Ga and implanting a significant K^+ density,[25] which enables a shorter chemical bath deposition of CdS (→ thinner CdS layer) to achieve the necessary surface passivation *and* inversion. Thinner CdS layers allow more < 530 nm photons to reach the CIGS absorber. The ZnO layer used in the cells also contributes to the reduction in the loss in the photo-

current. Replacing ZnO with wider bandgap (ZnMg)O improved the EQE further. For the present champion 22.9% CIGS cell, Cs was added as alkali metal[26]. The shape of the normalized EQE of the standard champion CIGS cell is now comparable to that of the c-Si cell. However, there is still photo-current loss due to the top TCO layer, a loss, common to all cells that use TCO windows. The V_{OC} and V_{MP} of the champion polycrystalline-CIGS cell, which has a bandgap, similar to that of c-Si, are now comparable to that of the latter (c.f. Table 1). Improvement in V_{OC} and V_{MP} of CIGS cells can happen by further reducing interface recombination and by making the back surface highly reflective.

Polycrystalline-CdTe: There has been rapid progress in polycrystalline CdTe-based solar cell PCE. When we compare EQEs of the champion cells (FIG. 4b), we find a similar trend as for CIGS cells, i.e., significant photo-current efficiency improvement for the higher energy photons correlates with PCE improvement. Particularly, the losses due to the CdS layer, used to create the p-n junction with CdTe (FIG. S9(b)), have been mostly eliminated and the EQE seems to be limited only by the optical absorption of the glass/TCO substrate at short wavelengths. A semiconductor bandgap can be changed by compositional changes. Though normally the change in bandgap is monotonic with change in composition, in certain cases there is a minimum badgap at an intermediate composition of the two constituents with different bandgaps. This phenomenon is called "bandgap bowing" and occurs in the Cd(Se_xTe_{1-x}) and $CdTe_{1-x}S_x$) systems. Based on the known 'bandgap bowing' effect in the $CdTe_{1-x}Se_x$/ $CdTe_{1-x}S_x$, systems, and reports suggesting $CdTe_{1-x}Se_X$ in 'First Solar' modules[27], it is highly likely that the absorber material in the present champion device is not neat CdTe, but $CdTe_{1-x}Se_x$ and/or $CdTe_{1-x}S_x$[28]. The efficiency improvement is possibly due to the bandgap grading in the poly-crystalline-CdTe technology where infiltration of Se in the absorber material produces $CdTe_{1-x}Se_x$, which, for low Se content, will extend optical absorbance to lower wavelengths. Being proprietary technologies, information about the process used to reduce the effect of CdS layer is not available in the public domain. However, similar works in academia suggest that a CdS:O layer may have been used to decrease the filtering effect and the use of CdSe (which can inter-diffuse with the top of the CdTe layer to form $CdTe_{1-x}S_x$) along with CdS layer also allows using a thinner CdS layer[29].

Though the photocurrent efficiency, J_{SC} is among the best of any cell type, V_{OC} losses remain. V_{OC} in CdTe cells can be > 1 V for single crystalline material with suitable interfacial materials[30]. In poly-crystalline material, minimization of non-radiative recombination at the grain-boundaries and in the grain bulk (due to defects) will increase η_{int}, which in turn can reduce the operating loss of the cell. In fact, polycrystalline-CdTe based cells have already shown Voc > 900 mV[31] due to reduction in the non-radiative recombination.

Sustainable chalcogenides ((CZTSS), Cu_2ZnSnS_4 (CZTS)): The sustainable chalcogenide thin-film-based solar cells have shown substantial progress in the past five years and their best PCE is now ~10%. Due to the similar ionic radii of Cu^+ and Zn^{+2} and the low formation energies for the neutral defect centers, the [Cu_{Zn}^-, Zn_{Cu}^+] defect complex is prevalent in CZTSS/CZTS. The experimentally observed broadening, which likely results from significant density of states into the gap, band tailing (FIG. 4c), will lead to a loss in V_{OC} of these cells [32]. The Urbach energy in these systems can be of the order of ~50 meV[33,34] which implies that even in the radiative limit, qV_{OC} is expected to be much lower than qV_{OC}^{SQ} , since $J_0^{Rad} >> J_0^{SQ}$.

Considering the effects of alkali ion treatment of the absorber layer in CIGS (initially with Na, nowadays with K and Cs), some such development may possible exist for the CZTS and CZTSS systems. However, such treatments cannot cancel effects of bulk static disorder. The defect centres produced due to sulphur vacancy[35] have a large cross section for carrier trapping and subsequent non-radiative recombination and are, hence, known as 'killer defects', which lower the voltage output of the cell even when present in small concentrations. Indeed, eliminating 'killer defects'[36] requires changes in the bulk of the materials, i.e., these are fundamental materials issues. It may be worth to look beyond the CdS/CZTS(S) interfaces to improve the photo-current efficiencies for the higher energy photons, since there is considerable loss in photocurrent due to the low EQE values <530 nm in champion devices (FIG. S10). Moreover, due to a 'cliff like' band offset at the CZTS/CdS interface, charge accumulation occurs which leads to non-radiative recombination of holes in the CZTS layer with the accumulated electrons in the CdS layer, which decreases η_{int} and results in the low V_{OC} of the cell $Zn_{1-x}Cd_xS$ appears to be a better choice than CdS, because its bandgap is wider and the band offset at the interface can be tuned by varying the Zn/Cd ratio. The immediate effect of switching to $Zn_{1-x}Cd_xS$ is apparent from the EQE of CZTSS cells in the sub-520 nm region (FIG. S10).

OTHER MATERIALS:

ABX_3 Metal Halide Perovskites: Solar cells, based on these absorbers, have shown very impressive progress in their PCE in the past 5 years, compared to the development of other PV technologies[37].The similarity in preparation of the polycrystalline thin films of these materials to methods, used for organic electronics and/or dye-sensitized cells on the one hand, and for other thin film absorbers, such as CIGS, on the other hand, helped drive a huge research effort, which undoubtedly contributed to the meteoric rise in the cell performances. In FIG. 4d, we show the evolution of the EQE of certified small area champion cells, which is high for high-energy photons even in the early cells, unlike what was the case for the CdTe and CIGS technologies. This is due, at least in part, to the use of a wide bandgap hole transport, electron-blocking selective contact (e.g., Spiro-OMeTAD) and an electron-transporting layer (esp. TiO_2) (FIG. S9c) with good transmittance for high energy photons, and to the fact that nearly all preparation methods yield materials with respectable diffusion

lengths[38,39]. The increase in absolute photocurrents over the years is well reflected in the improved EQE values near the band edge (FIG. 4d), the result of efficient photon absorption. Part of this "optical" improvement is due to a shift from films with small crystalline domains (few tens nm infiltrated into porous scaffold), to films with larger polycrystalline domains (100s nm to microns). For the latter, the extinction coefficient near the band edge is greatly enhanced due to reduced disorder in the excitonic absorption transition. The improved absorption in the red region of the spectrum can also be ascribed to improved crystalline quality of the absorber (decrease in trap-assisted recombination), which has enabled thicker films to operate well. The photocurrent further improved due to use of slightly lower bandgap ABX_3 materials that result from having cation mixtures on the A site, and specifically a transition to formamidinium-rich compositions, often with mixed halides on the X site.

Though high densities of native defects are expected for halide perovskites, prepared at low temperatures, there is no clear experimental evidence for such, which may be explained by defect healing[40] and/or suggested defect tolerance [41,42]. The Urbach energies, which are a measure of the presence, energy distribution and density, of electronic states in the bandgap region, for polycrystalline ABX_3 approach those of c-GaAs and c-Si.[43,44] We show the evolution of the *OL* from past to present small area champion cells (FIG 4(e)). From the Figure we see that improvement in cell performance is reflected in decreased operational loss. The contact materials appear to contribute significantly to the OL. It has been argued that the voltage efficiency of these cells can be like that of GaAs, based on η_{int} > ~90% for *ABX_3 films* after certain molecular chemical surface passivation of such films[45]. While a necessary condition for reducing OL, what matters is η_{ext} *of the complete cell,* which poses the challenge to make *interfaces* from/with optimized *surfaces* to make cells. Control over interfacial recombination may be achieved by reducing the interfacial contact between the charge recombination layer and the electrical contact layer.

a-Si: There is almost no progress in PV technology of hydrogenated amorphous Si, often denoted as a-Si:H (we use here "a-Si") in the last decade, as far as the actual conversion efficiency is concerned. Presumably, this lack of progress has its cause at least partly in to intrinsic material limitations of the a-Si absorber (due to its static disorder). This technology has the highest OL among all those we consider here. Already some 3.5 decades ago it was shown that the presence of tail states in an amorphous semiconductor, such as a-Si, implies several 100s of mV additional voltage loss in the system[46]; we submit that this intrinsic loss (in part shared with CZTS(S)) is a bigger obstacle for market penetration than the much-studied initial intrinsic instability of the material, the so-called Staebler-Wronski effect. We do note however, that a-Si is important for high efficiency c-Si SHJ cells, and although it is not playing the "central role", the past developments in a-Si have enabled the present world record c-Si efficiency, a nice example of cross-fertilization between PV technologies.

Quantum dot solar cells: In these types of cells the charge transport between the quantum do (QDs) has been a problem since the QD surfaces are often covered with higher bandgap or insulating organic ligands. The presence of defects on QD surfaces also lowers the achievable photovoltage. Liu *et al*. showed that capping the PbS QDs with $[PbX_3]^-/[PbX]^+$ (X= halide) instead of typical organic cations/ anions reduces the tail states in the QDs,[47] and solar cells with them showed improved photo-voltage. Swarnkar *et al*. used $CsPbI_3$ perovskite QDs to prepare cells with PCE > 10%[48]. In these cells, QDs are capped with long alkyl chain ligands, which hinder charge transport between the QDs. To improve the charge transport across the $CsPbI_3$ QDs Sanehira *et al*.[49] added a small amount of formamidinium iodide (FAI) to $CsPbI_3$ QD arrays, which decreased the interparticle distance, leading to improved charge transport and yielding the impressive top PCE for these cells; based on this achievement we see that there is now considerable room for further photocurrent efficiency improvement. It is debate-able if ABX_3 halide perovskites simply engulfed the QD field (traditionally based on III-V or metal chalcogenide semiconductors), or if QDs remain a discrete technology.

Organic photovoltaics (OPV): The PCE of the certified 1 cm^2 champion single junction device is now at 11.2 %, which has progressed from <10% values in a decade. The present champion device (area = ~1cm^2) uses a donor-acceptor type polymer: [6,6]- phenyl-C71-butyric acid methyl ester (PC70BM) bulk heterojunction as active layer[50]. The relatively poor voltage efficiency in an OPV has origins both in charge separation and recombination. Part of the absorbed energy is used (and lost, in terms of photovoltage) to separate charges at the donor-acceptor interface and form the charge trans-fer (CT) states, which arise due to the interaction of the donor and acceptor molecules. Although these CT states are photoactive, they generate negligible photocurrent. E_g^{PV} is mainly determined by the absorbance profile of the lower bandgap material between the Donor (D) and Acceptor (A) that form the heterojunction. CT states add more electronic states to those already present, due to electronic dis-order of D and A material. Both absorption strength of CT states and their position (E_{CT}) with respect to the E_g^{PV} affect the voltage output of the cell. Thus, a key to improve the voltage efficiency is to minimize $|E_{CT} - E_g^{PV}|$ and minimizing photon absorption by CT states via smart design of materials, e.g. using *non-fullerene based* acceptors.[51]

Over the years, the voltage efficiency of OPVs (non-certified) improved by bringing the energy of the charge transfer states, E_{CT} and E_g^{PV} closer (FIG. 5 (a) and 5(b) and S11). This improvement in voltage efficiency is mainly due to decreasing the loss factor, $kTln\left(\frac{J_0^{Rad}}{J_0^{SQ}}\right)$, the 5th loss term in eq. (5).. The reduction in non-radiative recombination (6th and 7th terms in eq. 5) is the additional cause for the im-proved OPV voltage efficiency. In OPV, non-radiative recombination at the D-A interface can be viewed as electron transfer in the *Marcus inverted regime* [52, 53]. Here, as the free energy of the pro-cess, given by E_{CT}, increases, the recombination rate decreases, which in turn increases the η_{ext} and results in higher voltage efficiency[53]. Energetic disorder at the interfaces and in the bulk, including

structural disorder[54,55] also add to the non-radiative recombination. In an organic blend, energy back transfer from the CT state to the Donor material can happen, which enables electron-hole recombination to proceed via electronic states of the pristine organic material[56]. In this scenario, if the donor material has high photoluminescence quantum yield, then non-radiative recombination can be further supressed. We note that the inherent presence of high energy vibrational modes (especially in the C=C bond, omnipresent in organic conductors) can lead to ~160 meV loss due to non-radiative recombination.[53,57]

TAIL STATES AND VOLTAGE EFFICIENCY:

An exponential decrease of density of electronic states from the band edges is seen in semiconductors. Here, we discuss to what extent these tail states influence the voltage output. We limit our discussion to the voltage, since in real devices the tail states produce negligible current (and have very little influence on the value of E_g^{PV}). Building on an earlier reported approach[58], we estimate the impact of the Urbach energy, E_U on the achievable photovoltage for materials with different E_g^{PV}. In FIG.5 (c) we give our estimates of qV_{OC}^{Rad} for E_g^{PV} (between 1–2 eV) as function of E_U: the decrease in qV_{OC}^{Rad} values is small (e.g., 10 meV for E_U = 15 meV) for E_U < kT, but increases rapidly once E_U values exceed kT.

.

c-Si, GaAs, InP, CdTe, ABX_3, and CIGS all have E_U < kT (FIG.5c and Table S4). This enables us to use the simplified equation 7, for estimating the V_{oc} or radiative efficiencies for these technologies with good accuracy. For technologies such as a-Si, CZTS and CZTSS the E_U values are >40 meV, leading to an additional loss of several hundred meV in the radiative limit. The band tailing in CZTS and CZTSS originates from the static disorder, which is inherent to these materials; even in their single crystals the E_U is >> kT[33]. This material property will severely limit the voltage efficiency of the cell as we have seen in the case of a-Si, and, unless it is shown not to be inherent to these materials, will limit these specific absorbers to low PCE.

In OPV cells, the EQE below E_g^{PV} has a contribution from the CT states as well as from energetic disorder that is inherent to the pristine materials (See SI). Also in the more voltage efficient cells we do not see any significant photocurrent due to the CT absorbance states, which indicates that either the oscillator strength of the CT states is very weak or their energies are so close to E_g^{PV} that we cannot distinguish absorbance due to such states. E_U values are around 40-50 meV for low voltage efficiency

cells but are close to or less than kT for the high voltage efficiency ones. Thus, a-Si like (static) disorder in OPVs is no longer a bottleneck, using E_U, which is now < kT (FIG. 5d) to quantify the energetic disorder.[56, 59]

SCALE-UP LIMIT:

Though the fundamental physics of a particular solar cell does not change during scaling up cell size, maintaining the electronic quality over large areas and achieving high manufacturing yields, to be able to build modules, requires the ability to fabricate large area cells, reproducibly. Scaling-up photovoltaics requires achieving the following progression: small area (<< 1 cm^2) cell → 1 cm^2 (or larger) cells → mini module (area < 500 cm^2) → large area module → commercial large area module. FIG. 6 a shows the progress in each category and subcategory. Most often the fill factor appears as the first bottleneck during scale-up from small to large area PV cells. In FIG. 6 b we show how FF values differ between small and large area cells. The transition from small area to 1 cm^2 cell should be quick, once control over material quality for 1 cm^2 area is achieved; after that things often become harder. We see room for significant further progress in esp. halide perovskite technologies, by improving the FF of these cells. For CdTe and OPV, the FF for large and small area cells are already quite similar.

Si technology shows the best scale-up performances among the technologies, as is to be expected, given > 6 decades of development. For each type of c-Si cell architecture, there is around 3-4% drop in efficiency from the champion laboratory cell to the commercial modules. The GaAs-based modules (certified) have comparable efficiency to that of c-Si (which have 15 times larger area), though the former has higher single cell efficiency. There have been very significant improvements in both module and laboratory cell efficiencies in CIGS and CdTe technologies in the recent years as well in the case of OPV and the emerging halide perovskite-based one. For these last ones progress from lab cells to modules is still far behind that of Si, which can be ascribed to the unprecedented single cell development (mainly by university groups) as there do not seem to be any (known) fundamental obstacles.

There have been very significant improvements in both module and laboratory cell efficiencies in CIGS and CdTe technologies in the recent years. As there is always a time lag for the transition from lab to commercial module fabrication and optimization, we expect that these technologies will follow the pattern of c-Si technology development, but with delay and, due to less intensive focused optimization efforts, with the possible exception of polycrystalline-CdTe (i.e., Cd(Te,Se)).

Outlook:

While we discussed mainly the scientific and technological efforts behind the evolution of the different solar cell technologies, economic cost factors, as well as local political will and global politics may have played a pivotal role in the development of a particular technology and this will remain the situation in the future. Increasing public awareness about the need for sustainable and clean energy sources certainly helped and will support interest in the solar cell R&D.

For the established solar cell categories where commercial modules are available (e.g. c-Si, CIGS and CdTe), all champion cell development was carried out by the relevant commercial companies, rather than in academic labs. We can expect the same to happen with those cell technologies that near commercialization, for which present cell development is dominated by academia.

The development in the single crystal-based devices and polycrystalline-CIGS and -CdTe occurred mostly via interface modification and/or change in device architecture, indicating that absorber material development in these types reached a plateau. A major development in the two commercial polycrystalline -technologies is that CdS has either been eliminated or alloyed, such that its presence no more exacts a price in current. Focused research on the interfaces and device architecture will further improve cell performances and may led to cross fertilization of concepts for the development in emerging technologies as we have seen for GaAs and GaInP, CIGS and CdTe technologies.

The progress in c-Si can come close the maximum possible PCE of 29%, which takes the intrinsic material property of Si into account. We expect that the c-Si cell technology with the IBC-SHJ architecture which is a scalable technology will reinforce its position as the market leader in the single junction cell category. At present, a *cell* with 79 cm^2 area already shows 26.7% efficiency and the 26.6 % cell has a (for other PV technologies amazing) 180 cm^2 area. Those cell results lead us to expect that module efficiency will also increase in the future. We expect only small progress in mc-Si technology as the HIT-IBC technology used in the champion c-Si cell may not be suitable for mc-Si due to the intrinsically lower carrier diffusion lengths in mc-Si than in c-Si.

GaAs technology has almost reached its voltage limit, though a little improvement in the photocurrent efficiency is expected. GaInP cells are mostly small (< 1 cm^2) area because they are used in concentrator cells. Possibly future work on larger area GaInP cells can tell if the contacts have a drastic effect on the OL or not. c-InP cell technology can catch up with the performance of GaAs and GaInP cells because of the similar electronic quality of the absorber and interfacial materials used in these technologies.

Significant improvements in both laboratory cell and module efficiencies in inorganic polycrystalline solar cell technologies in the recent years have happened mainly due to the development of interfacial

materials. Better control of these charge collecting interfaces will result in higher PCE. There is always a time lag for the transition from the lab to commercial module fabrication and optimization, and we expect that the thin-film technologies will follow the pattern of c-Si technology development, but with delay and, due to less intensive focused optimization efforts, with the possible exception of polycrystalline-CdTe (or Cd(Te,Se).

In halide perovskite technologies, there is a need to decrease the operational loss for the standard 1 cm^2 cells. While overshadowed by the achievements of very small lab cells, the improvements in stabilities and in increasing cell area are as impressive and should pave the path to modules with higher PCE.. Within this assessment, we have only focussed on the fundamental properties of single junction PV cells. However, metal halide perovskites are highly suited for multi-junction approaches due to their compositionally tuneable band gap. When combined with c-Si, this has already led to a 28% 1cm^2 certified perovskite-on-silicon tandem efficiency[60], which is likely to be a technologically relevant approach. The eventual commercial viability of this technology will depend on the long-term stability under realistic conditions

The rapid progress of other thin film technologies, based on CdTe and CIGS, and the emergence of halide perovskites as PV materials, all of which yield better optoelectronic quality materials than a-Si, will likely discourage further R&D in a-Si technology. Thus, it would seem that significant development regarding materials and/or device structure, or identifying a unique market, will be needed for progress in a-Si technology. Though the certified record efficiency for a single junction OPV cell with area ≥ 1cm^2 remains at 11.3%, a small area (0.04 cm^2) cell has been reported with 15.6%, indicating rapid progress in the OPV technology[61]. However, cells including the innovations that yield E_U values below or around the critical 'kT threshold', which lead to the high voltage efficiency, are yet to be certified. The $E_g^{PV} - E_{CT}$ value and the E_U appear to be correlated. If there is any connection between them, many other D-A combinations can be designed for OPV. Based on the recent progress in the OPV materials development, we expect rapid improvements in the record efficiencies for OPV over the next few years. The prevalence of electronic defects in CZTS and CZTSS, which appears to be inherent in these materials, will limit their development and may make them obsolete.

The earth-abundance and the availability (which are not the same!) of elements required for the various PV technologies, differ significantly. If we limit ourselves to the PV active, absorber materials, then it is hard to beat Silicon, even if including its dopants. Using 10^6 atoms of Si as the reference, following Haxel et. al. [62] and setting 0.1 atoms per 10^6 Si atoms as an, admittedly arbitrary limit, In, Se, Cd and I closer to this limit though Te is challenging.

Concerning environmental issues of PV technologies, it is clear that appropriate considerations and deployment strategies must be investigated and adopted. Two of the elements, used in a commercial and an emerging thin film PV technology are Cd, in CdTe, and Pb, in metal-halide perovskite PV

cells, respectively raise ecotoxicity concerns. Extensive work with CdTe, in the past 15 years (primarily driven by First Solar), has established a safe means to manufacture, deploy and recycle CdTe PV modules[63]. The very low solubility product of CdTe in water naturally also minimizes the danger of groundwater contamination by Cd.

Pb-based halide perovskite PV is a much younger technology. However, initial life cycle analysis has revealed that the toxicological impact of lead is likely to be less than 0.3% of the total ecotoxicity impact of manufacturing and deploying Pb-based halide perovskite-on-silicon PV modules, even with the unrealistic boundary condition that all the Pb is eventually leached into the environment[64]. However, to gain full certitude as to the safe manufacture, use and end of life disposal of metal-halide perovskite PV modules, a large substantiated body of evidence is required to understand the full life cycle.

For OPV and to some extent for the ABX_3 halide perovskites (and other organic materials used in the cells) environmental effects of solvents used in the preparation, need to be considered, as well.

For a more balanced and complete view of the environmental impact of PV, we note that commonly used materials, such as indium, in ITO and even Si in Si PV cells, also carry an environmental impact, largely due to the energy cost of mining and/or purifying such materials

Based on today's and predicted future markets, technologies can become an alternative for c-Si and mc-Si, or complement then, only if production yields and stabilities of the technologies are comparable. A likely near-term future technology is that of affordable Si tandem cells, which may well become commercial within a few years, by fabricating a wider gap cell on top of a Si cell, to overcome the SQ single junction efficiency limit, with comparable lifetime and minimal added cost. The champion certified tandem cells, based on GaAs-on-Si, are with area < $5cm^2$ with most around 1 cm^2. Because the future of c-Si modules will be based on large area cells, metal halide perovskite-based cells appear key contenders for top cells for the tandem application. Also, recent improvements in (decreasing) operational losses for OPV cells and impressive improvements in OPV tandem cells[65], present OPV as well as possible viable top cells.

Figure Captions:

Figure 1: (a) Components of the operational loss (inspired by Hirst et al. [66]). The dotted vertical line marks the E_g^{PV}. The filled rectangles represent various losses associated with a real cell. The shaded rectangles represent the power output. (b) qV_{OC} versus the PV gap. The relationship between qV_{OC}^{SQ} and E_g^{PV} is quasi-linear for the normal solar cells with 1e V $\leq E_g^{PV} \geq$ 2.5 eV. The open circles are for the calculated qVoc values for different $\eta_{ext}$where $qV_{OC}^{SQ} = qV_{OC}^{Rad}$. The green dots are for the small area cells (< 1 cm^2). (c) Squares: Experimental operational loss vs. the PV gap; red squares for ≥ 1 cm^2 cells (aperture area or designated illumination area), green squares for < 1 cm^2 area cells. Black dots: Theoretical maximum operational loss, as calculated from the thermodynamic considerations in the SQ limit. (d) Voltage loss ($\Delta V = V_{OC}-V_{MP}$) for operation at maximum power. The empty black dots show the expected ΔV for a given open circuit voltage for ideal contacts and only radiative recombination. Empty blue dots show the expected ΔV for ideal contacts with a diode ideality factor n=2. The filled red dots (green dots for small area cells) show actual ΔV in the real devices. MPP: maximum power point. Other abbreviations are as in Table 1.

Figure 2: (a) Photon and carrier management with η_{int} =1 and 100% reflecting back surface (b) system with non-radiative recombination and parasitic absorbance at the back surface. The curvy blue and green arrows represent the incoming photons and photons generated due to the recombination of carriers, respectively. Yellow and black straight arrows show the propagation of electrons (filled red ovals) and holes (black ovals), respectively. NR = non-radiative recombination. (c) Schematic layout for a c-GaAs cell and (d) c-InP cell.

Figure 3: Schematic device architectures for different types of champion c-Si cells. The curly arrows show the direction of the sunlight. (a) Passivated emitter with rear locally diffused (PERL) cell with both front and back contacts (record PCE = 25 %; ref [67]) with p:c-Si as the absorber (b) A inter-digitated back contact (IBC) homojunction solar cell with interdigitated p^+ and n^+ diffused regions in the Si substrate which are directly contacted by the hole and electron contacts, respectively. The top surface is passivated by the creation of a front surface field. (record PCE = 25.2 %; ref[68]) (c) Top and bottom contacted Heterojunction with Intrinsic Thin-layer (SHJ) cell. The p^+ and n^+ heterojunctions are created near to the front and back surfaces, respectively. The transparent conducting oxides (TCOs) act both as an electrode and as an anti-reflection coating (record PCE = 25.1%; ref. [69]). (d) SHJ-IBC cell (hybridization of device concepts outlined in (b) and (c)) with inter-digitated p^+ and n^+ heterojunction layers contacted by hole- and electron-collecting electrodes, respectively (record PCE = 26.7%; ref [17,70]). The front of the n-type: c-Si wafer surface is textured (not shown in the figure.) to minimize reflection and is passivated with a-Si.

Figure 4: (a) External quantum efficiency (EQE) (sourced from the solar cell efficiency tables by Green et. al. [61]).for the recent champion CIGS ($CuIn_XGa_{1-X}Se$) cells; (b) same for CdTe ($CdTe_{1-X}Se_X$) cells. The The vertical dotted green line represents the bandgap of CdS, a commonly used buffer layer in both these cells. (c) Disorder-induced band gap broadening in CZTS and CZTSS (d) Evolution of the EQE of small area champion ABX_3 perovskite devices (areas generally ≤ 0.2 cm^2). Normalised EQEs are rescaled to match the reported J_{SC} values of the cells (e) Evolution of the operational loss in small area ABX_3 devices (green squares). The 3.8%[71], 9.7%[72] and 10.7%[73] data are for early cells, and were not certified.

Figure 5: Distribution of band gaps and Electroluminescence (EL) spectra of (a) P3HT:PCBM[74], (b) P3TEA: SFPDI2 [75]. The deviation from SQ limit decreases as separation between the EL spectrum and E_g^{PV} decreases. (See also FIG S11). (c) qV_{OC}^{Rad} and E_U for different E_g^{PV}. The decrease in qV_{OC}^{Rad} is drastic when E_U >kT. The dots represent the expected qV_{OC}^{Rad} for different technologies based on their E_g^{PV} and typical E_U (see Table S4) associated with them (d) Log (EQE) as function of excitation energy, from which E_U associated with different OPVs (See SI and FIG. S12), is calculated. Cells with E_U close to kT show high voltage efficiency and only exponential decay of states

Figure 6: (a) PCE of minicell, standard cell, and modules for various types solar cells (b) Fill factor (FF) for champion cells of the different PV technologies; the values for small area cells are represented by green squares. The references for the FF values of large area cells are the same as provided in Table1. The references for FF values for small area cells are CZTSS[76], CZTS[77],OPV[18] and ABX_3[78]. The calculated FF values are based on the equation,

$$FF = \frac{v'_{OC} - \ln(v'_{OC} - \ln(v'_{OC}+1)+1)}{v'_{OC}} \times \frac{v'_{OC} - \ln(v'_{OC}+1)}{v'_{OC} - \ln(v'_{OC}+1)+1},$$

see section '*Relation of Fill Factor (FF) with V_{OC}*' in SI for the derivation and also ref [79] for an empirical formula) as a function of the V_{OC} for different values of the ideality factor, n (which can be extracted from the dark I-V curve).

Table 1:

PV gap, E_g^{PV} of each technology, experimentally determined V_{OC} and V_{MP} values, operational loss (OL) values: (E_g^{PV}-qV$_{OC}$), (E_g^{PV}-qV$_{MP}$), (qV$_{OC}$/E_g^{PV}), (qV$_{MP}$ / E_g^{PV}), (qV_{MP}^{Ideal} / E_g^{PV}) and loss due to contacts, of the best (reported) laboratory cells. Note that the Eg^{PV} values deviate slightly for some materials from their ($\frac{d}{dE}EQE$), which is shown in brackets in Column 2.

Cell type	E_g^{PV} [eV] ($\frac{d}{dE}EQE)_{Max}$ [eV]	V_{OC} [V]	V_{MP} [V]	E_g^{PV}-qV$_{OC}$ [eV]	OL, E_g^{PV}-qV$_{MP}$ [eV]	qV$_{OC}$ /E_g^{PV} [%]	qV$_{MP}$/ E_g^{PV} [%]	qV_{MP}^{Ideal}/ E_g^{PV} [%]	Loss from contacts [mV] [b]	Ref. [c]
c-Si	1.10 (1.07)	0.74	0.66	0.36	0.44	67	60	71	1	[77]
GaAs	1.42 (1.41)	1.13	1.02	0.29	0.40	80	72	75	14	[61]
InP	1.38 (1.34)	0.94	0.82	0.44	0.56	68	59	75	30	[77]
[a] GaInP	1.88 (1.84)	1.46	1.36	0.42	0.52	78	72	79	1	[68]
mc-Si	1.11 (1.09)	0.67	0.57	0.44	0.54	60	51	71	20	[80]
$CdTe_{1-x}Se_x$	1.42 (1.42)	0.88	0.74	0.54	0.68	62	52	75	52	[81]
CIGS	1.12 (1.12)	0.74	0.63	0.38	0.49	66	56	71	27	[18]
CZTSS	1.13 (1.14)	0.53	0.39	0.60	0.74	47	34	72	68	[61]
CZTS	1.48 (1.46)	0.71	0.54	0.77	0.94	48	36	76	88	[77]
ABX_3	1.55 (1.55)	1.12	0.90	0.43	0.65	72	58	77	125	[78]
a-Si	1.77 (1.71)	0.90	0.73	0.87	1.04	51	41	78	81	[81]
OPV (Toshiba)	1.62 (1.63)	0.78	0.64	0.84	0.98	48	41	77	55	[81]
[a]QD	1.77 (1.78)	1.16	0.95	0.61	0.82	65	54	78	114	[49]

[a] area < 1cm^2, c = (single) crystalline , mc= multi-crystalline, a = amorphous; CIGS = Cu(In,Ga)Se_2, CZTSS = $Cu_2ZnSnS_{4-y}Se_y$, CZTS = Cu_2ZnSnS_4, ABX_3 = Halide Perovskite, QD = quantum dot. [c] references for the EQE values, current-voltage curves used for the calculation of E_g^{PV} values, and for solar cell parameters, respectively; [b] includes loss due to non-ideal (n > 1) recombination.

Table 2:
PV Gap, E_g^{PV} of each technology, maximum possible photo current density, J_{SC}^{SQ} in SQ limit, experimental photo-current density, J_{SC}, current density at maximum power point, J_{MP}, and the ratios between J_{SC}^{SQ} , J_{SC} and J_{MP}

Cell type	PV Gap, E_g^{PV} [eV]	J_{SC}^{SQ} mA.cm^{-2}	J_{SC} mA.cm^{-2}	J_{MP} mA.cm^{-2}	J_{SC}/J_{SC}^{SQ} [%]	J_{MP}/J_{SC}^{SQ} [%]	J_{MP}/J_{SC} [%]
c-Si	1.10	44.2	42.6	40.3	96	91	95
GaAs	1.42	32.0	29.8	28.5	93	89	96
InP	1.38	33.7	31.1	29.6	92	88	95
[a] GaInP	1.88	17.4	16.3	15.8	94	91	97
mc-Si	1.11	44.1	41.1	39.1	93	89	95
$CdTe_{1-x}Se_x$	1.42	32.0	30.2	28.3	94	88	94
CIGS	1.12	43.8	38.8	36.4	89	83	94
CZTSS	1.13	43.4	33.6	29.1	77	67	87
CZTS	1.48	29.6	21.8	18.7	74	63	86
ABX_3	1.55	27.3	24.9	22.2	91	84	89
a-Si	1.77	20.4	16.4	13.9	80	68	85
OPV Toshiba	1.62	24.8	19.3	17.3	78	70	90
[a] QD	1.77	20.3	15.2	14	75	69	92

[a] area < 1 cm^2; J_{SC}^{SQ} calculated from global AM1.5 spectrum (ASTM G-173-03 global, sourced from ref.[82]) Abbreviations are as in Table 1. Max. $\frac{d}{dE}EQE$ values are given in Table 1. References for the current-voltage curves, used to calculate the J_{SC} and J_{MP} values, are given in Table 1.

References:

1. Shockley, W. & Queisser, H. J. Detailed Balance Limit of Efficiency of p□n Junction Solar Cells. *J. Appl. Phys.* **32,** 510–519 (1961).
2. Nayak, P. K., Bisquert, J. & Cahen, D. Assessing possibilities and limits for solar cells. *Adv. Mater.* **23,** 2870–2876 (2011).
3. Nayak, P. K. & Cahen, D. Updated Assessment of Possibilities and Limits for Solar Cells. *Adv. Mater.* **26,** 1622–1628 (2014).
4. Rau, U., Blank, B., Müller, T. C. M. & Kirchartz, T. Efficiency Potential of Photovoltaic Materials and Devices Unveiled by Detailed-Balance Analysis. *Phys. Rev. Appl.* **7,** 044016

(2017).

5. Wang, Y. *et al.* Optical Gaps of Organic Solar Cells as a Reference for Comparing Voltage Losses. *Adv. Energy Mater.* **8,** 1801352 (2018).
6. Markvart, T. The thermodynamics of optical étendue. *J. Opt. A Pure Appl. Opt.* **10,** 015008 (2008).
7. Hirst, L. C. & Ekins-Daukes, N. J. Fundamental losses in solar cells. *Prog. Photovoltaics Res. Appl.* **19,** 286–293 (2011).
8. Miller, O. D., Yablonovitch, E. & Kurtz, S. R. Strong Internal and External Luminescence as Solar Cells Approach the Shockley–Queisser Limit. *IEEE J. Photovoltaics* **2,** 303–311 (2012).
9. Rau, U. Reciprocity relation between photovoltaic quantum efficiency and electroluminescent emission of solar cells. *Phys. Rev. B* **76,** 085303 (2007).
10. Schnitzer, I., Yablonovitch, E., Caneau, C. & Gmitter, T. J. Ultrahigh spontaneous emission quantum efficiency, 99.7% internally and 72% externally, from AlGaAs/GaAs/AlGaAs double heterostructures. *Appl. Phys. Lett.* **62,** 131–133 (1993).
11. Green, M. A. Radiative efficiency of state-of-the-art photovoltaic cells. *Prog. Photovoltaics Res. Appl.* **20,** 472–476 (2012).
12. Sheng, X. *et al.* Device Architectures for Enhanced Photon Recycling in Thin-Film Multijunction Solar Cells. *Adv. Energy Mater.* **5,** 1400919 (2015).
13. Geisz, J. F., Steiner, M. A., García, I., Kurtz, S. R. & Friedman, D. J. Enhanced external radiative efficiency for 20.8% efficient single-junction GaInP solar cells. *Appl. Phys. Lett.* **103,** 041118 (2013).
14. Bandgap of GaInP can be tuned by stoichiometry (Ga/In ratio) and/or by degree of structural ordering (see the references below).
15. Steiner, M. A. *et al.* CuPt ordering in high bandgap GaxIn1-xP alloys on relaxed GaAsP step grades. *J. Appl. Phys.* **106,** 063525 (2009).
16. Wanlass, M. Systems and Methods for Advanced Ultra-High-Performance InP Solar Cells. (2017). at <http://www.freepatentsonline.com/y2015/0280042.html>
17. Yoshikawa, K. *et al.* Silicon heterojunction solar cell with interdigitated back contacts for a photoconversion efficiency over 26%. *Nat. Energy* **2,** 17032 (2017).
18. Green, M. A. *et al.* Solar cell efficiency tables (version 52). *Prog. Photovoltaics Res. Appl.* **26,** 427–436
19. Taguchi, M. *et al.* 24.7% Record Efficiency HIT Solar Cell on Thin Silicon Wafer. *IEEE J. Photovoltaics* **4,** 96–99 (2014).
20. Richter, A., Hermle, M. & Glunz, S. W. Reassessment of the Limiting Efficiency for Crystalline Silicon Solar Cells. *IEEE J. Photovoltaics* **3,** 1184–1191 (2013).
21. Trupke, T., Zhao, J., Wang, A., Corkish, R. & Green, M. A. Very efficient light emission from bulk crystalline silicon. *Appl. Phys. Lett.* **82,** 2996–44107 (2003).

22. Yang, Y. M. *et al.* Development of high-performance multicrystalline silicon for photovoltaic industry. *Prog. Photovoltaics Res. Appl.* **23,** 340–351 (2015).
23. Macdonald, D. & Geerligs, L. J. Recombination activity of interstitial iron and other transition metal point defects in p- and n-type crystalline silicon. *Appl. Phys. Lett.* **85,** 4061–4063 (2004).
24. Benick, J. *et al.* High-Efficiency n-Type HP mc Silicon Solar Cells. *IEEE J. Photovoltaics* **7,** 1171–1175 (2017).
25. Chiril˘, A. *et al.* Potassium-induced surface modification of Cu(In,Ga)Se 2 thin films for high-efficiency solar cells. *Nat. Mater.* **12,** (2013).
26. Wu, J.-L., Hirai, Y., Kato, T., Sugimoto, H. & Bermude, V. New World Record Efficiency up to 22.9% for Cu(In,Ga)(Se,S)2 Thin-Film Solar Cells. in *7th World Conference on Photovoltaic Energy Conversion (WCPEC-7)* (2018). at <http://www.wcpec7.org/eWCPEC/mobile/show_presentation.php?abstractno=154>
27. EDS Newsletters | IEEE Electron Devices Society. (2017).
28. Poplawsky, J. D. *et al.* Structural and compositional dependence of the CdTexSe1−x alloy layer photoactivity in CdTe-based solar cells. *Nat. Commun.* **7,** 12537 (2016).
29. Paudel, N. R., Poplawsky, J. D., Moore, K. L. & Yan, Y. Current Enhancement of CdTe-Based Solar Cells. *IEEE J. Photovoltaics* **5,** 1492–1496 (2015).
30. Zhao, Y. *et al.* Monocrystalline CdTe solar cells with open-circuit voltage over 1 v and efficiency of 17%. *Nat. Energy* **1,** 16067 (2016).
31. Gloeckler, M., Sankin, I. & Zhao, Z. CdTe solar cells at the threshold to 20% efficiency. *IEEE J. Photovoltaics* **3,** 1389–1393 (2013).
32. Gokmen, T., Gunawan, O., Todorov, T. K. & Mitzi, D. B. Band tailing and efficiency limitation in kesterite solar cells. *Appl. Phys. Lett.* **103,** 103506 (2013).
33. Ng, T. M. *et al.* Optoelectronic and spectroscopic characterization of vapour-transport grown Cu2ZnSnS4single crystals. *J. Mater. Chem. A* **5,** 1192–1200 (2017).
34. Yan, C. *et al.* Beyond 11% Efficient Sulfide Kesterite $Cu_2Zn_xCd_{1-x}SnS_4$ Solar Cell: Effects of Cadmium Alloying. *ACS Energy Lett.* **2,** 930–936 (2017).
35. Kim, S., Park, J. S. & Walsh, A. Identification of Killer Defects in Kesterite Thin-Film Solar Cells. *ACS Energy Lett.* **3,** 496–500 (2018).
36. Kim, S., Park, J.-S. & Walsh, A. Identification of Killer Defects in Kesterite Thin-Film Solar Cells. *ACS Energy Lett.* **3,** 496–500 (2018).
37. Snaith, H. J. Present status and future prospects of perovskite photovoltaics. *Nat. Mater.* **17,** 372–376 (2018).
38. Stranks, S. D. *et al.* Electron-hole diffusion lengths exceeding 1 micrometer in an organometal trihalide perovskite absorber. *Science (80-.).* **342,** 341–344 (2013).
39. Edri, E. *et al.* Elucidating the charge carrier separation and working mechanism of CH3NH3PbI3−xClx perovskite solar cells. *Nat. Commun.* **5,** 3461 (2014).

40. Ceratti, D. R. *et al.* Self-Healing Inside APbBr3Halide Perovskite Crystals. *Adv. Mater.* **30,** 1706273 (2018).
41. Brandt, R. E., Stevanovic, V., Ginley, D. S. & Buonassisi, T. Identifying defect-tolerant semiconductors with high minority-carrier lifetimes: Beyond hybrid lead halide perovskites. *MRS Commun.* **5,** 265–275 (2015).
42. Zakutayev, A. *et al.* Defect tolerant semiconductors for solar energy conversion. *Journal of Physical Chemistry Letters* **5,** 1117–1125 (2014).
43. De Wolf, S. *et al.* Organometallic Halide Perovskites: Sharp Optical Absorption Edge and Its Relation to Photovoltaic Performance. *J. Phys. Chem. Lett.* **5,** 1035–1039 (2014).
44. Sutter-Fella, C. M. *et al.* Band Tailing and Deep Defect States in CH3NH3Pb(I1-xBrx)3Perovskites As Revealed by Sub-Bandgap Photocurrent. *ACS Energy Lett.* **2,** 709–715 (2017).
45. Braly, I. L. *et al.* Hybrid perovskite films approaching the radiative limit with over 90% photoluminescence quantum efficiency. *Nat. Photonics* 1 (2018). doi:10.1038/s41566-018-0154-z
46. Tiedje, T. Band tail recombination limit to the output voltage of amorphous silicon solar cells. *Appl. Phys. Lett.* **40,** 627–629 (1982).
47. Liu, M. *et al.* Hybrid organic–inorganic inks flatten the energy landscape in colloidal quantum dot solids. *Nat. Mater.* **16,** 258–263 (2017).
48. Swarnkar, A. *et al.* Quantum dot-induced phase stabilization of α-CsPbI3 perovskite for high-efficiency photovoltaics. *Science* **354,** 92–95 (2016).
49. Sanehira, E. M. *et al.* Enhanced mobility $CsPbI_3$ quantum dot arrays for record-efficiency, high-voltage photovoltaic cells. *Sci. Adv.* **3,** eaao4204 (2017).
50. Mori, S. *et al.* Organic photovoltaic module development with inverted device structure. in *Materials Research Society Symposium Proceedings* **1737,** 26–31 (Cambridge University Press, 2015).
51. Yan, C. *et al.* Non-fullerene acceptors for organic solar cells. *Nature Reviews Materials* **3,** 18003 (2018).
52. Marcus, R. A. Electron transfer reactions in chemistry. Theory and experiment. *Rev. Mod. Phys.* **65,** 599–610 (1993).
53. Benduhn, J. *et al.* Intrinsic non-radiative voltage losses in fullerene-based organic solar cells. *Nat. Energy* **2,** 17053 (2017).
54. Nayak, P. K., Garcia-Belmonte, G., Kahn, A., Bisquert, J. & Cahen, D. Photovoltaic efficiency limits and material disorder. *Energy Environ. Sci.* **5,** 6022 (2012).
55. Nayak, P. K. *et al.* The effect of structural order on solar cell parameters, as illustrated in a SiC-organic junction model. *Energy Environ. Sci.* **6,** 3272 (2013).
56. Qian, D. *et al.* Design rules for minimizing voltage losses in high-efficiency organic solar

cells. *Nat. Mater.* **17,** 703–709 (2018).

57. Chen, X. K. & Brédas, J. L. Voltage Losses in Organic Solar Cells: Understanding the Contributions of Intramolecular Vibrations to Nonradiative Recombinations. *Adv. Energy Mater.* **8,** 1702227 (2018).
58. Jean, J. *et al.* Radiative Efficiency Limit with Band Tailing Exceeds 30% for Quantum Dot Solar Cells. *ACS Energy Lett.* **2,** 2616–2624 (2017).
59. Venkateshvaran, D. *et al.* Approaching disorder-free transport in high-mobility conjugated polymers. *Nature* **515,** 384–388 (2014).
60. Perovskite world record | Oxford PV. at <https://www.oxfordpv.com/news/oxford-pv-perovskite-solar-cell-achieves-28-efficiency>
61. Green, M. A. *et al.* Solar cell efficiency tables (Version 53). *Prog. Photovoltaics Res. Appl.* **27,** 3–12 (2019).
62. Haxel, G. B., Hedrick, J. B. & Orris, G. J. *Rare earth elements: critical resources for high technology: US Geological Survey fact sheet 087-02. Technical report, US Geological Survey* (2002). at <https://pubs.usgs.gov/fs/2002/fs087-02/>
63. Chuangchote, S. *et al.* Review of Environmental, Health and Safety of CdTe Photovoltaic Installations throughout Their Life-Cycle. (2012). at <http://www.firstsolar.com/-/media/First-Solar/Sustainability-Documents/Sustainability-Peer-Reviews/Thai-EHS-Peer-Review_EN.ashx>
64. Latest News - CHEOPS. at <https://www.cheops-project.eu/news-in-brief/first-results-regarding-the-environmental-impact-of-perovskitesilicon-tandem-pv-modules>
65. Meng, L. *et al.* Organic and solution-processed tandem solar cells with 17.3% efficiency. *Science (80-.).* **361,** eaat2612 (2018).
66. Ekins-Daukes, N. J. & Hirst, L. C. Fundamental Losses in Solar Cells. in *24th European Photovoltaic Solar Energy Conference, 21-25 September 2009, Hamburg, Germany* 457–461 (WIP-Munich, 2009). doi:10.4229/24THEUPVSEC2009-1CV.4.11
67. Green, M. A., Emery, K., Hishikawa, Y., Warta, W. & Dunlop, E. D. Solar cell efficiency tables (version 40). *Prog. Photovoltaics Res. Appl.* **20,** 606–614 (2012).
68. Green, M. A., Emery, K., Hishikawa, Y., Warta, W. & Dunlop, E. D. Solar cell efficiency tables (version 47). *Prog. Photovoltaics Res. Appl.* **24,** 3–11 (2016).
69. Adachi, D., Hernández, J. L. & Yamamoto, K. Impact of carrier recombination on fill factor for large area heterojunction crystalline silicon solar cell with 25.1% efficiency. *Appl. Phys. Lett.* **107,** 233506 (2015).
70. Green, M. A. *et al.* Solar cell efficiency tables (version 50). *Prog. Photovoltaics Res. Appl.* **25,** 668–676 (2017).
71. Kojima, A., Teshima, K., Shirai, Y. & Miyasaka, T. Organometal halide perovskites as visible-light sensitizers for photovoltaic cells. *J. Am. Chem. Soc.* **131,** 6050–1 (2009).

72. Kim, H.-S. *et al.* Lead Iodide Perovskite Sensitized All-Solid-State Submicron Thin Film Mesoscopic Solar Cell with Efficiency Exceeding 9%. *Sci. Rep.* **2,** 591 (2012).
73. Lee, M. M., Teuscher, J., Miyasaka, T., Murakami, T. N. & Snaith, H. J. Efficient hybrid solar cells based on meso-superstructured organometal halide perovskites. *Science* **338,** 643–7 (2012).
74. Gong, W. *et al.* Influence of energetic disorder on electroluminescence emission in polymer: Fullerene solar cells. *Phys. Rev. B - Condens. Matter Mater. Phys.* **86,** 024201 (2012).
75. Liu, J. *et al.* Fast charge separation in a non-fullerene organic solar cell with a small driving force. *Nat. Energy* **1,** 16089 (2016).
76. Green, M. A., Emery, K., Hishikawa, Y., Warta, W. & Dunlop, E. D. Solar cell efficiency tables (version 44). *Prog. Photovoltaics Res. Appl.* **22,** 701–710 (2014).
77. Green, M. A. *et al.* Solar cell efficiency tables (version 50). *Prog. Photovoltaics Res. Appl.* **25,** 668–676 (2017).
78. Green, M. A. *et al.* Solar cell efficiency tables (version 51). *Prog. Photovoltaics Res. Appl.* **26,** 3–12 (2018).
79. Green, M. A. Accuracy of analytical expressions for solar cell fill factors. *Solar Cells* **7,** 337–340 (1982).
80. Green, M. A. *et al.* Solar cell efficiency tables (version 51). *Prog. Photovoltaics Res. Appl.* **26,** 3–12 (2018).
81. Green, M. A., Emery, K., Hishikawa, Y., Warta, W. & Dunlop, E. D. Solar cell efficiency tables (Version 45). *Prog. Photovoltaics Res. Appl.* **23,** 1–9 (2015).
82. Solar Spectral Irradiance: Air Mass 1.5. at <https://rredc.nrel.gov/solar//spectra/am1.5/#about>

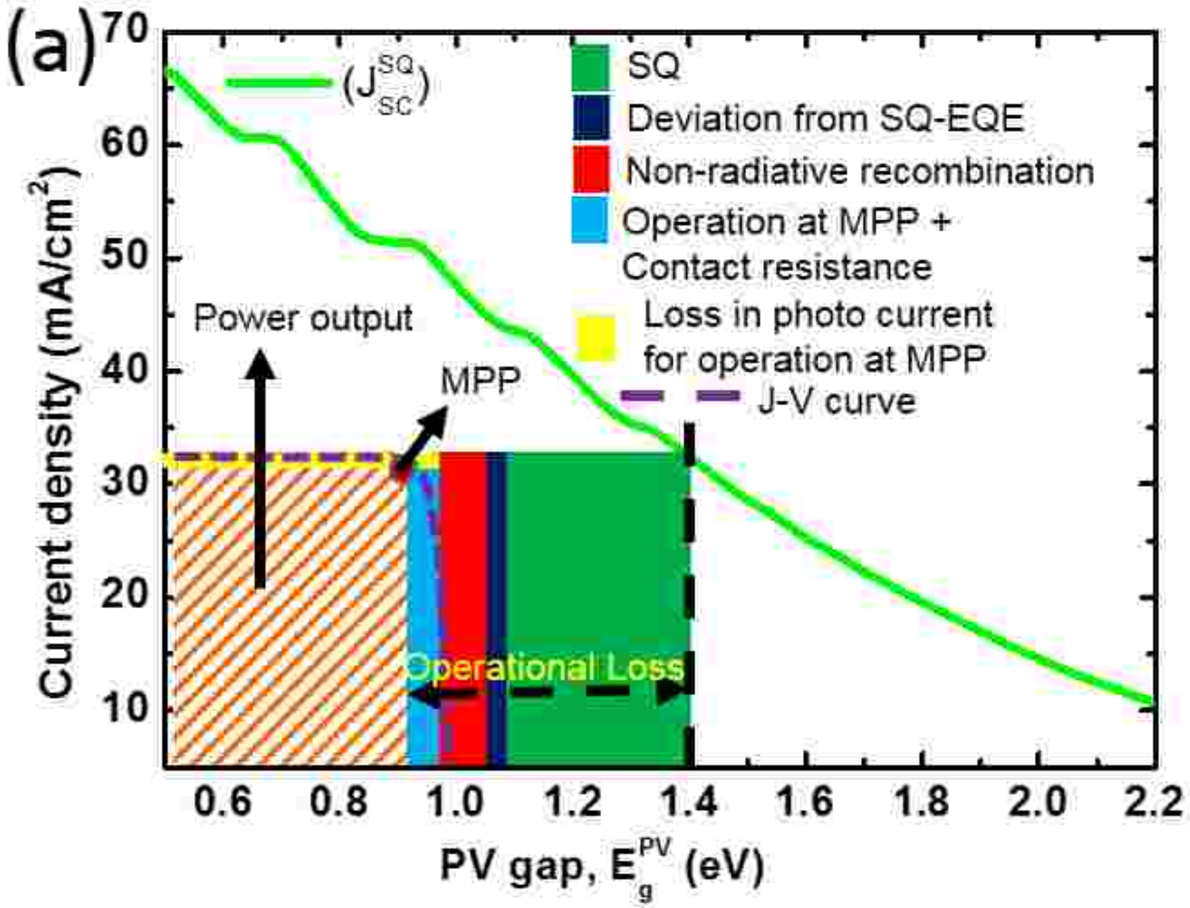
(a)
Current density (mA/cm²)
PV gap, E_g^PV (eV)
(J_SC^SQ)
SQ
Deviation from SQ-EQE
Non-radiative recombination
Operation at MPP + Contact resistance
Loss in photo current for operation at MPP
J-V curve
Power output
MPP
Operational Loss

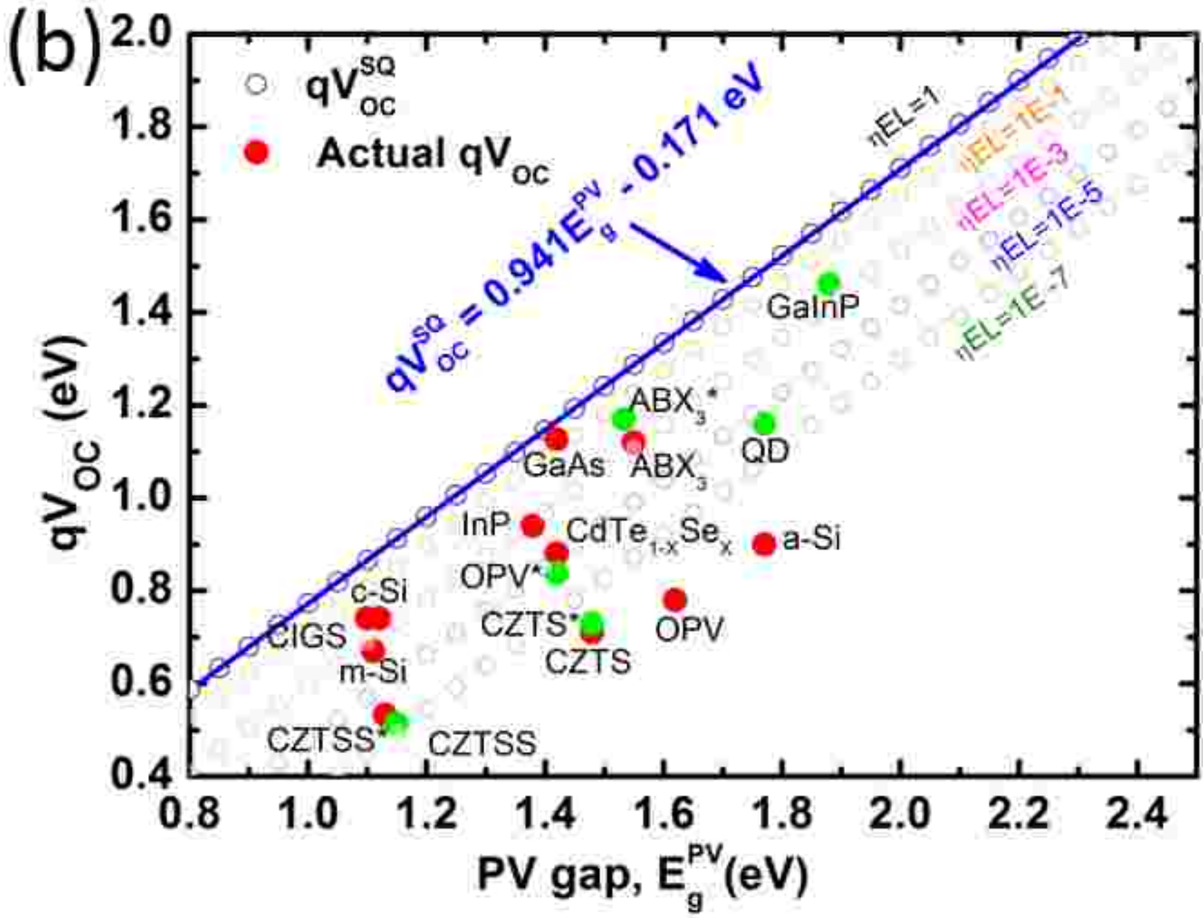
(b)
qV_OC^SQ
Actual qV_OC
qV_OC^SQ = 0.941E_g^PV - 0.171 eV
ηEL=1
ηEL=1E-1
ηEL=1E-3
ηEL=1E-5
ηEL=1E-7
qV_OC (eV)
PV gap, E_g^PV(eV)
GaInP
ABX3*
ABX3
QD
GaAs
InP
CdTe1-xSex
a-Si
OPV*
OPV
c-Si
CZTS*
CZTS
CIGS
m-Si
CZTSS*
CZTSS

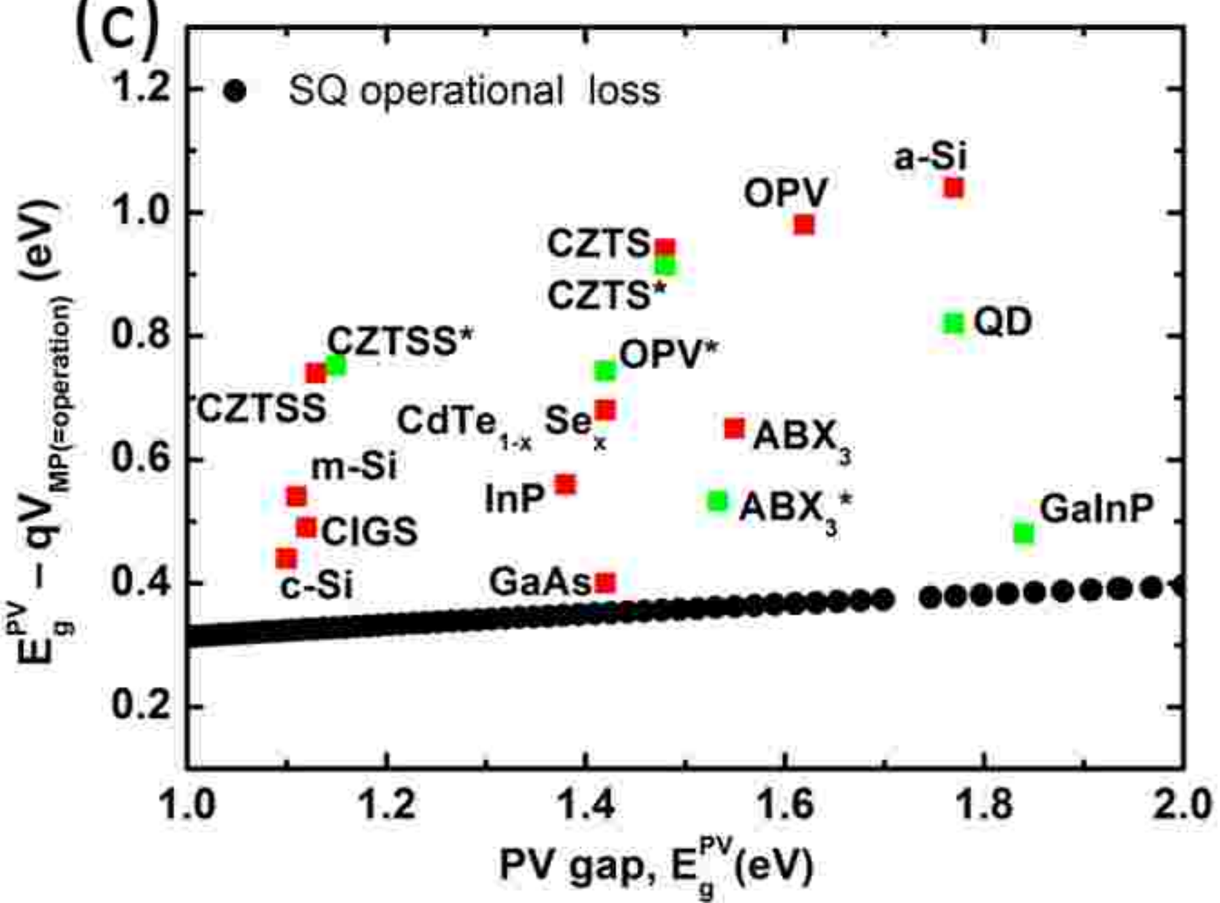
(c)
SQ operational loss
E_g^PV − qV_MP(=operation) (eV)
PV gap, E_g^PV(eV)
a-Si
OPV
CZTS
CZTS*
QD
CZTSS*
OPV*
CZTSS
CdTe1-xSex
ABX3
m-Si
InP
ABX3*
GaInP
CIGS
c-Si
GaAs

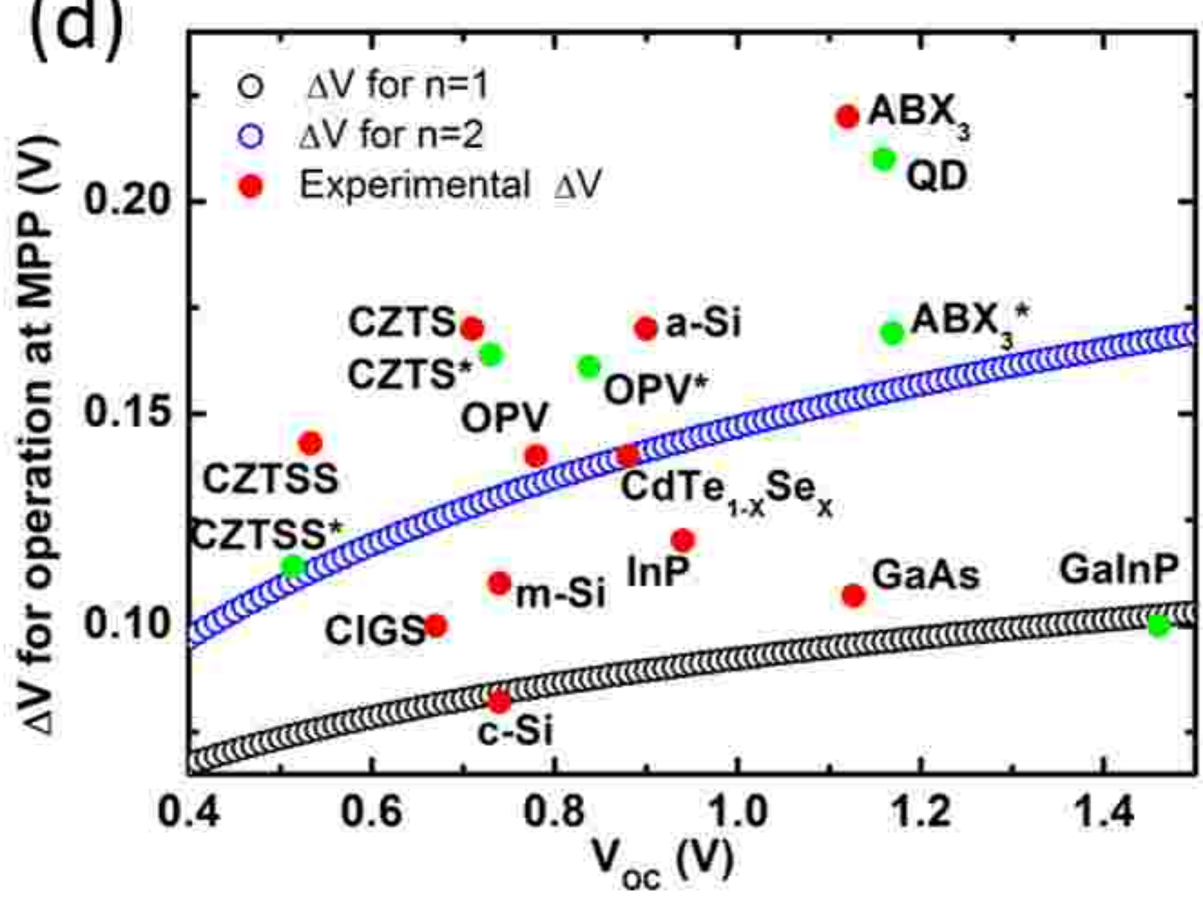
(d)
ΔV for n=1
ΔV for n=2
Experimental ΔV
ΔV for operation at MPP (V)
V_OC (V)
ABX3
QD
CZTS
CZTS*
a-Si
ABX3*
OPV
OPV*
CZTSS
CZTSS*
CdTe1-xSex
InP
GaAs
GaInP
m-Si
CIGS
c-Si

(a)

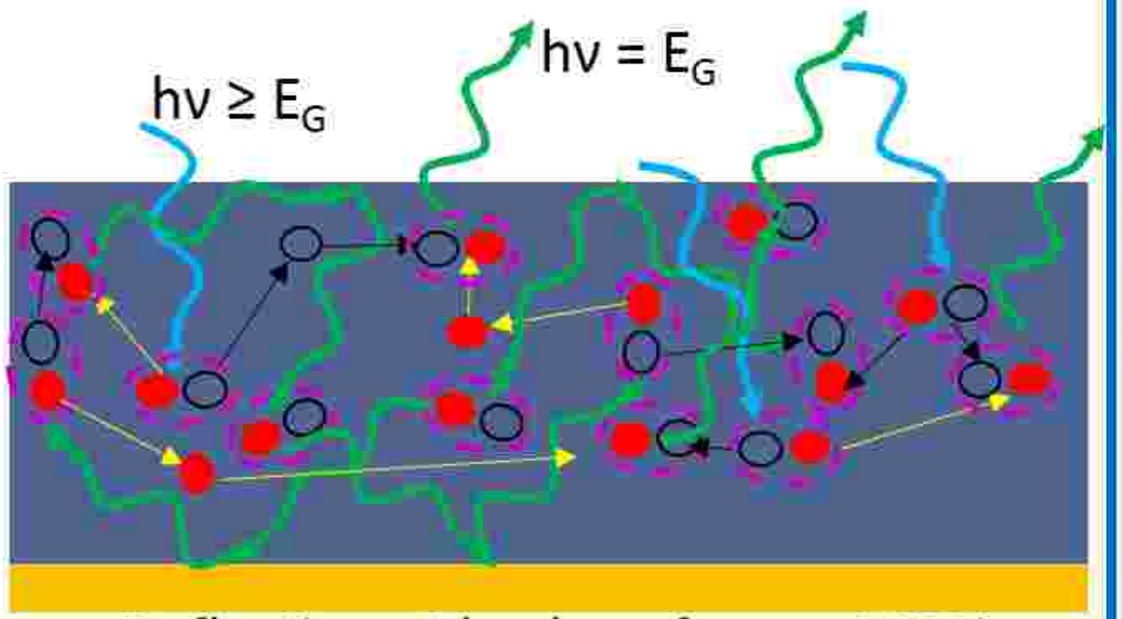

Reflection at back surface = 100%

(b)

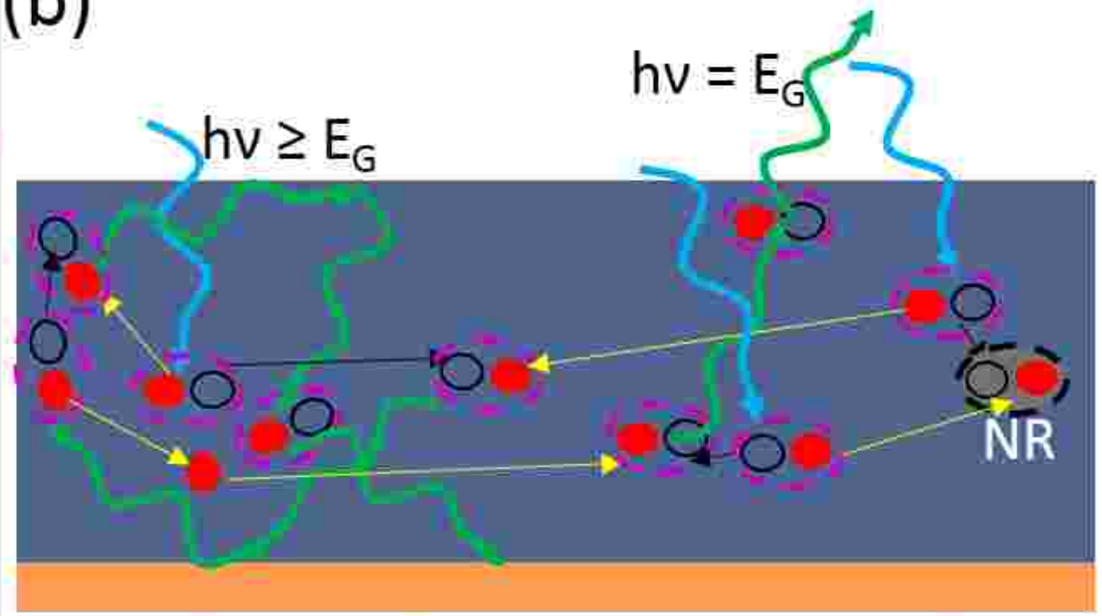

Reflection at back surface < 100%

(c)

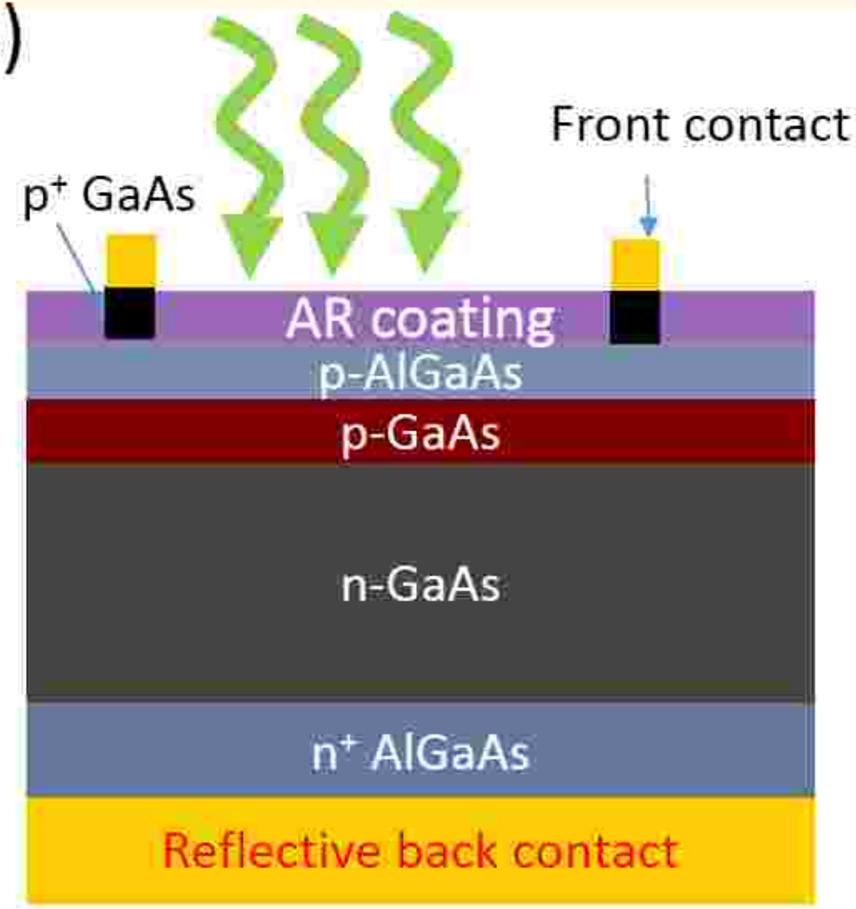

(d)

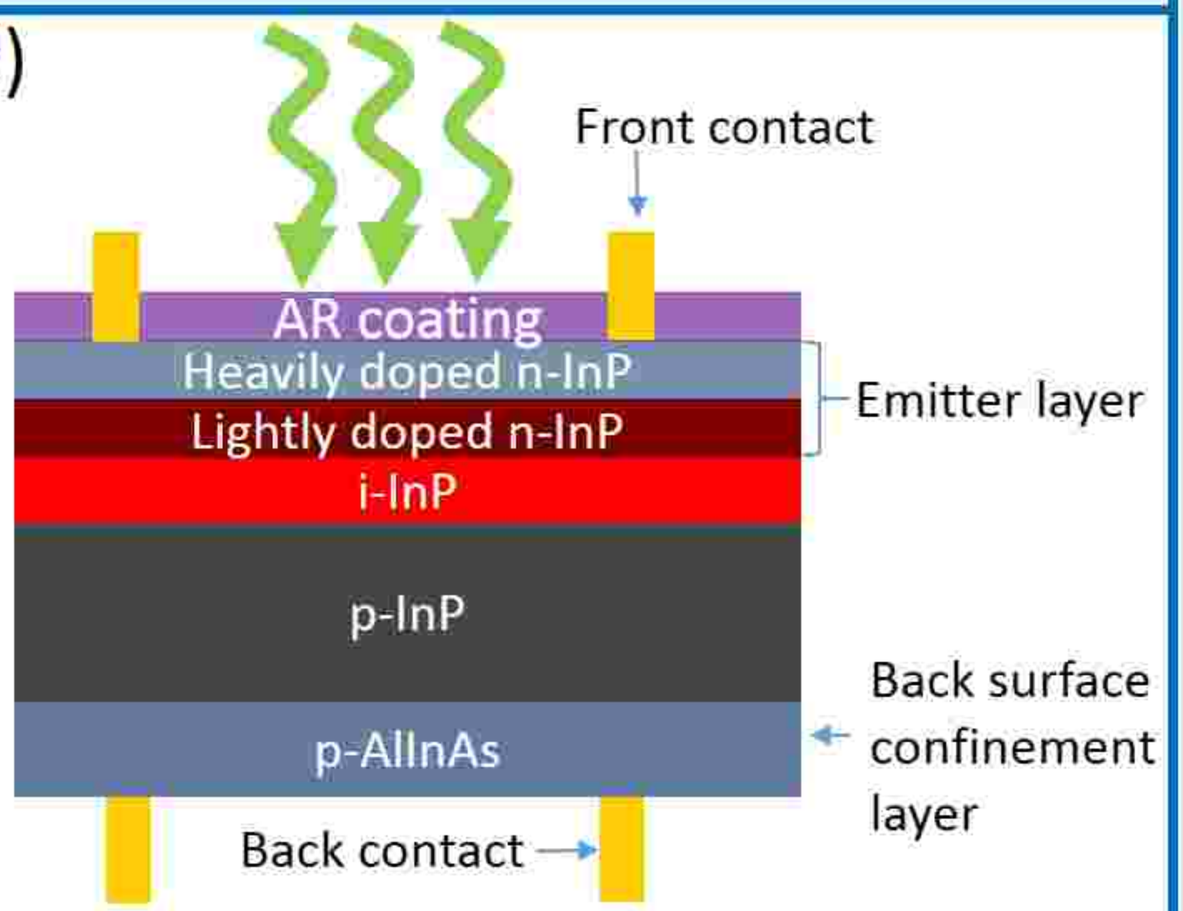

(a)

PERL

'Inverted' pyramids

Front electrode

AR coating

Oxide passivation

n^+

p:c-Si

n

p^+

Absorber

Oxide passivation

Back electrode

(b)

IBC

AR coating

Front surface

Field passivation

n:c-Si

n^+

p^+

Absorber

Rear Passivation

Rear electrodes

(c)

SHJ

Front Electrode

TCO

p:a-Si

i:a-Si

n:c-Si

Absorber

i:a-Si

n:a-Si

Back electrode

(d)

IBC-SHJ

AR coating

Passivated

front surface

n:c-Si

Absorber

n: a-Si

p: a-Si

i:a-Si

Rear electrodes

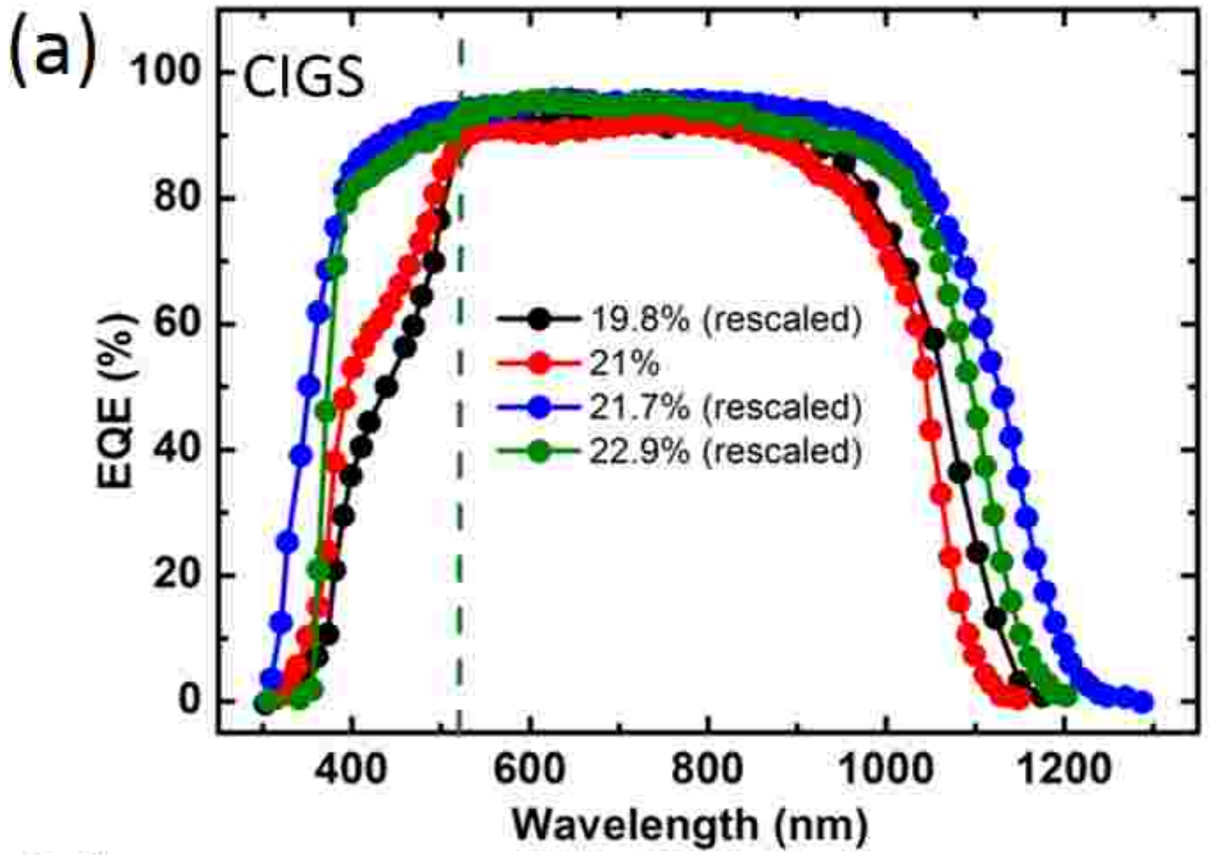
(a)
CIGS
EQE (%)
Wavelength (nm)
19.8% (rescaled)
21%
21.7% (rescaled)
22.9% (rescaled)

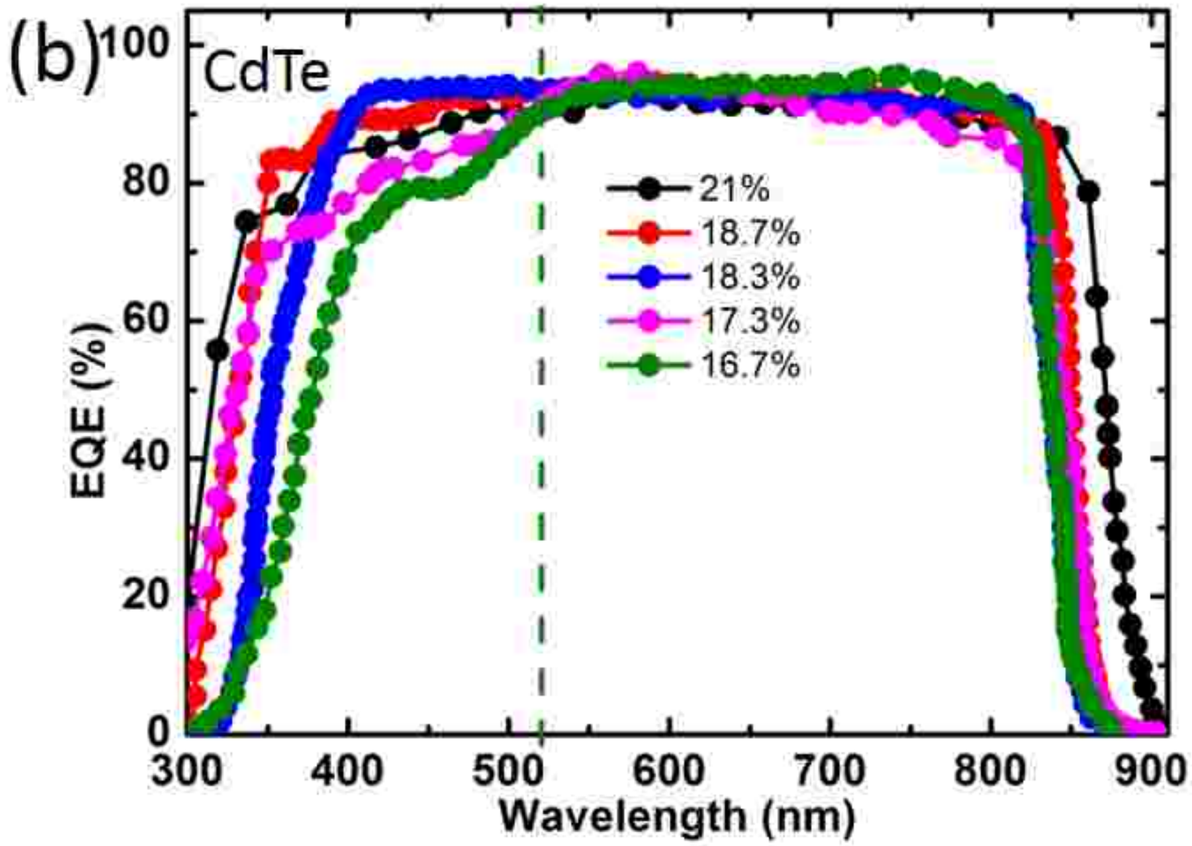
(b)
CdTe
EQE (%)
Wavelength (nm)
21%
18.7%
18.3%
17.3%
16.7%

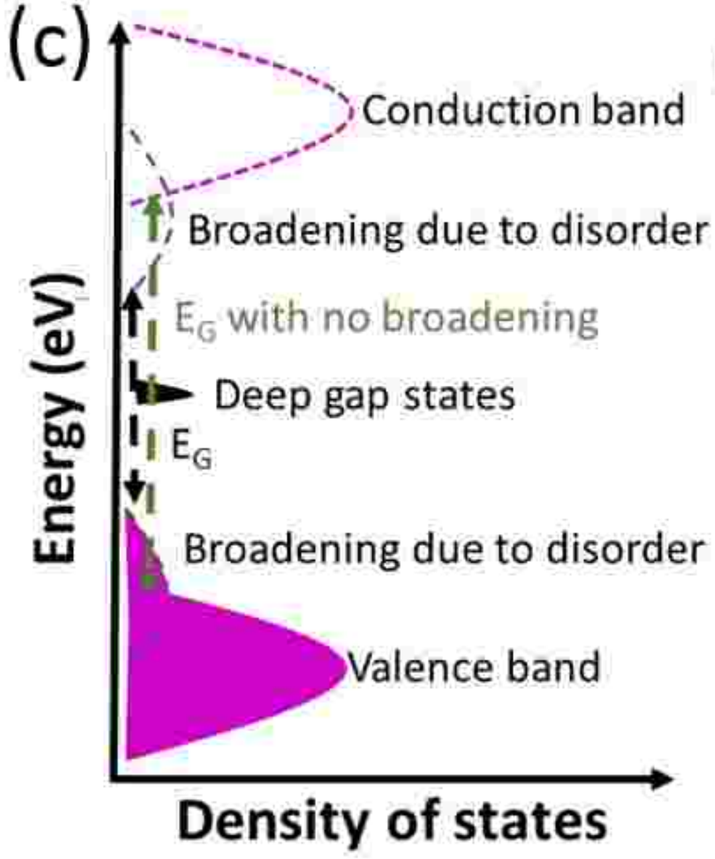
(c)
Conduction band
Broadening due to disorder
E_G with no broadening
Deep gap states
E_G
Broadening due to disorder
Valence band
Energy (eV)
Density of states

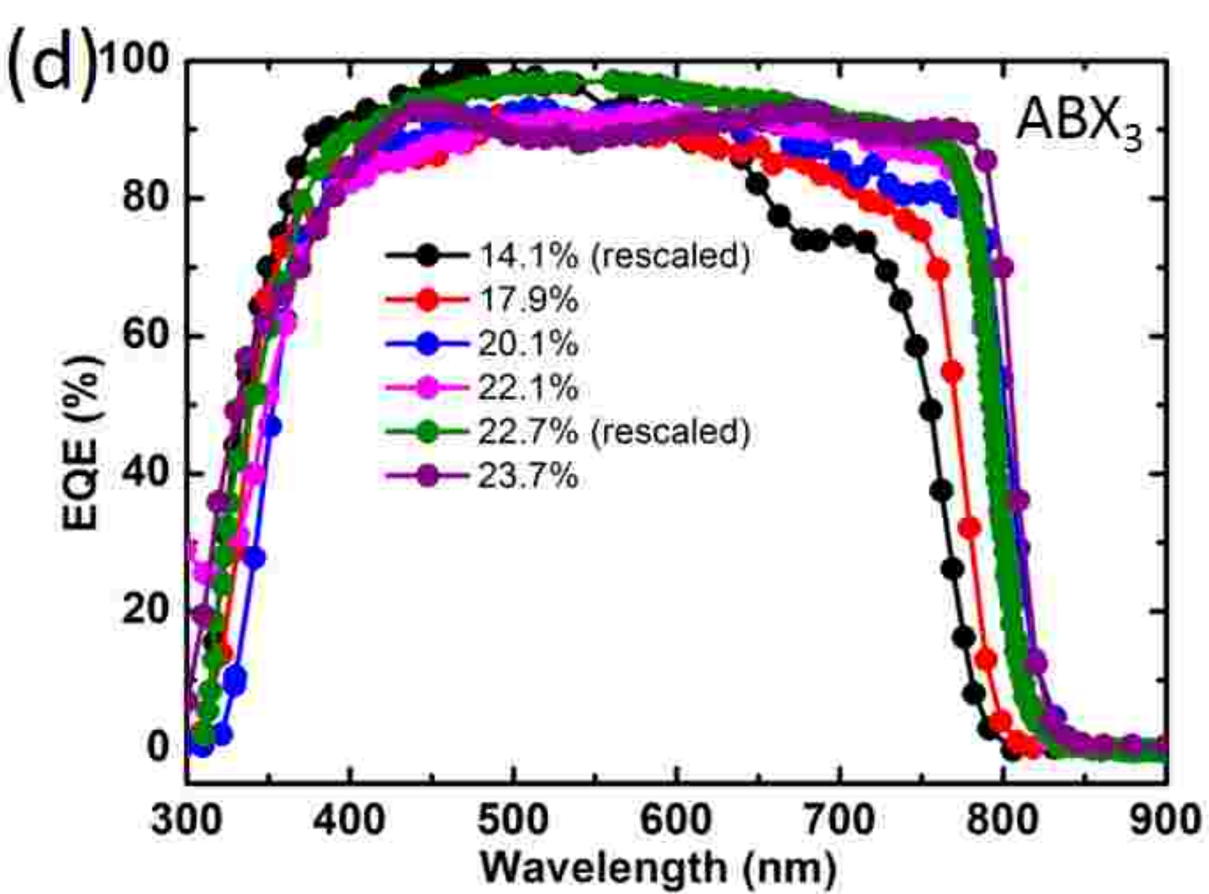
(d)
ABX3
EQE (%)
Wavelength (nm)
14.1% (rescaled)
17.9%
20.1%
22.1%
22.7% (rescaled)
23.7%

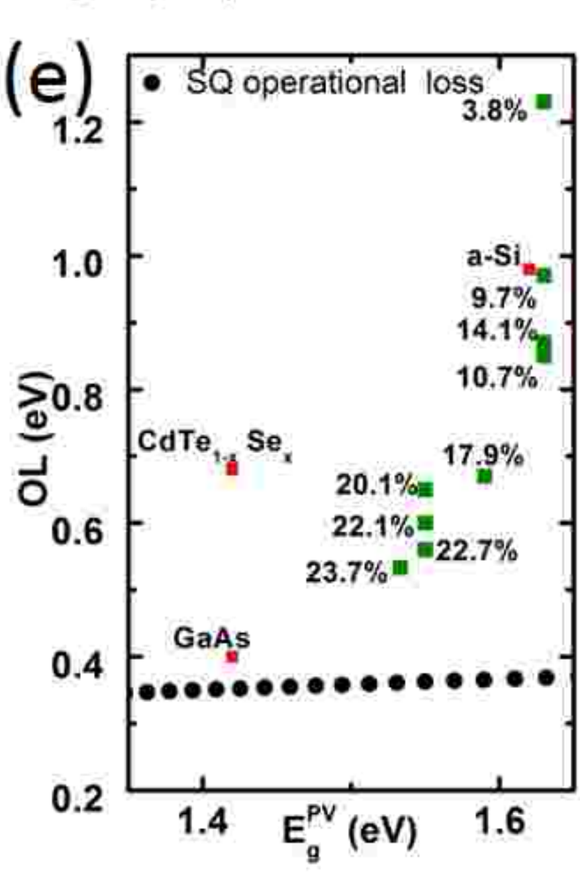
(e)
SQ operational loss
3.8%
a-Si
9.7%
14.1%
10.7%
CdTe1-xSex
17.9%
20.1%
22.1%
22.7%
23.7%
GaAs
OL (eV)
E_g^PV (eV)

(a)

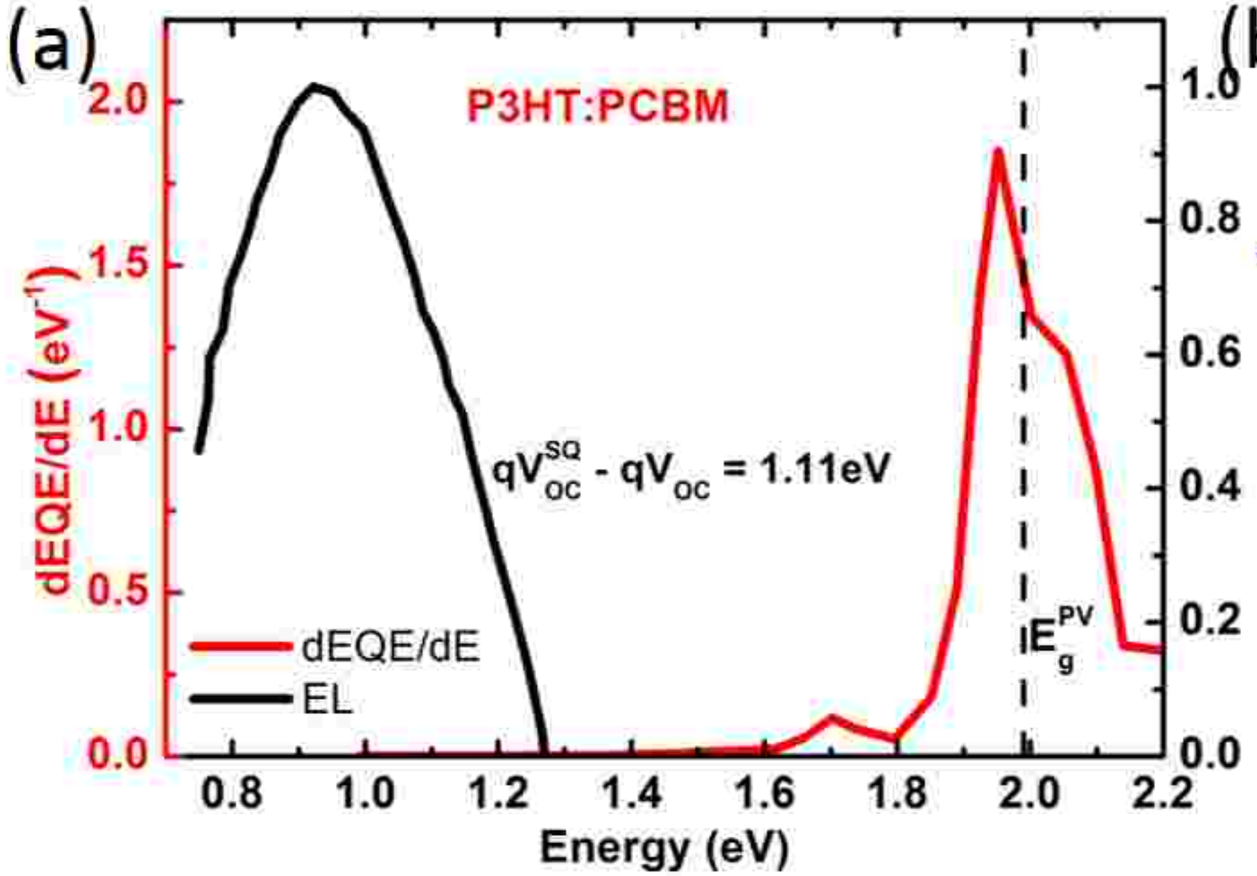
P3HT:PCBM
dEQE/dE
EL
$qV_{OC}^{SQ} - qV_{OC}$ = 1.11eV
E_g^{PV}
dEQE/dE (eV^{-1})
Energy (eV)

(b)

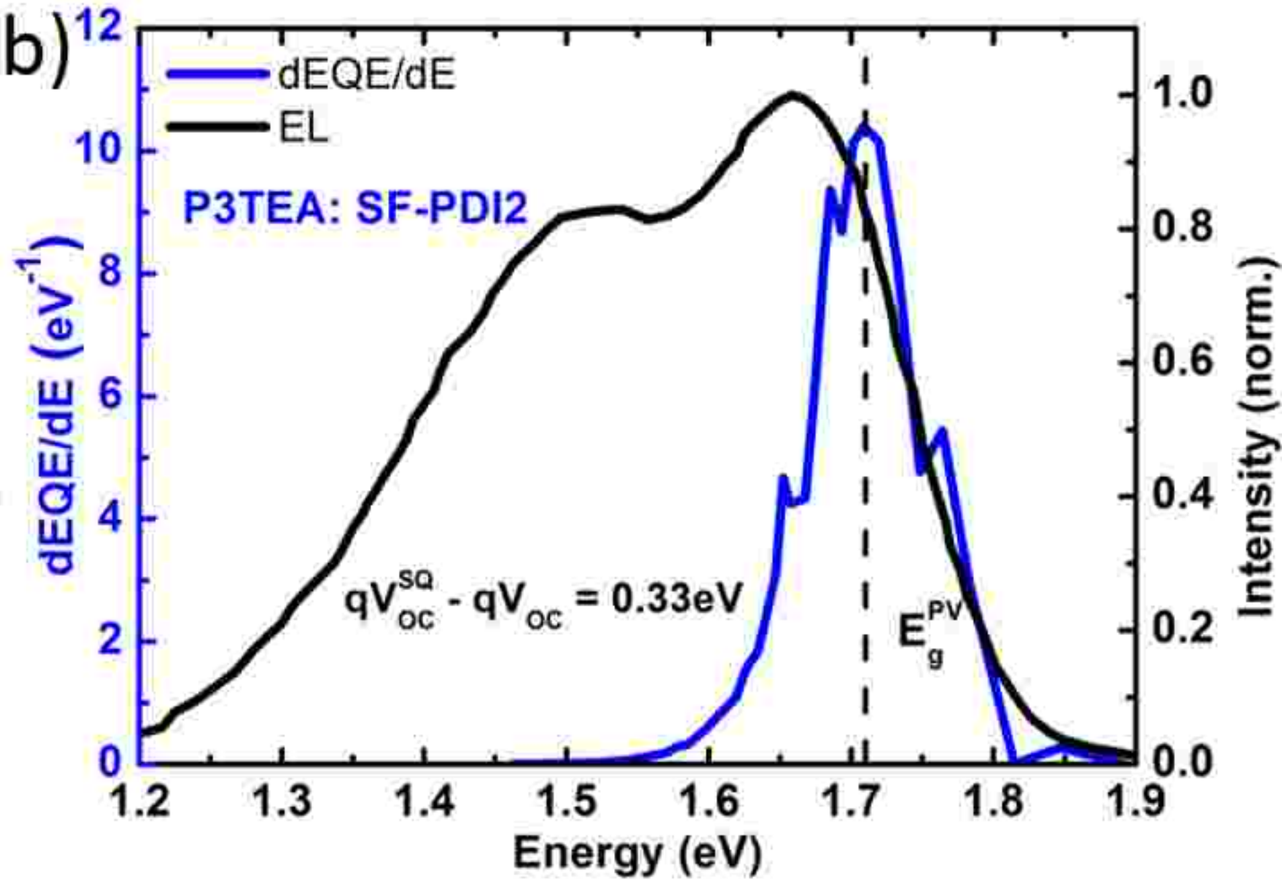
dEQE/dE
EL
P3TEA: SF-PDI2
$qV_{OC}^{SQ} - qV_{OC}$ = 0.33eV
E_g^{PV}
dEQE/dE (eV^{-1})
Intensity (norm.)
Energy (eV)

(c)

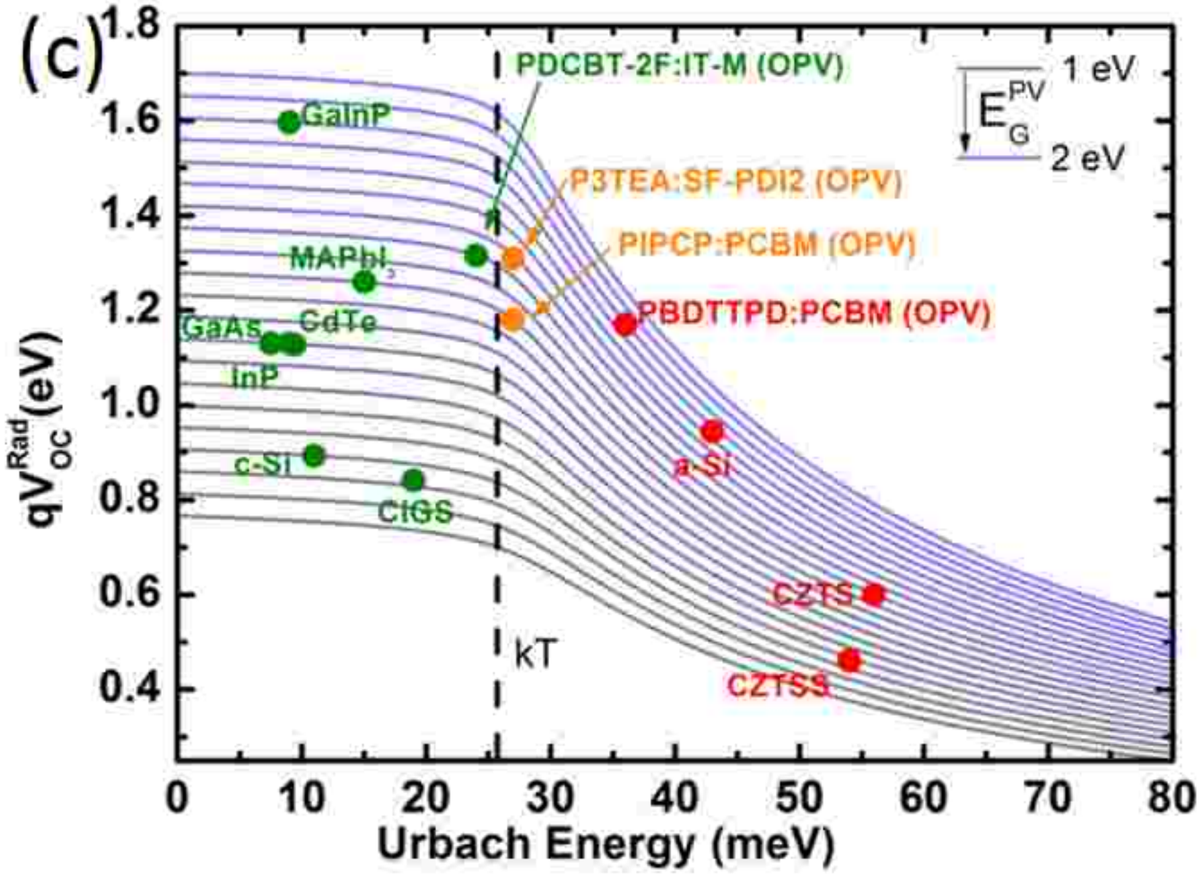
PDCBT-2F:IT-M (OPV)
P3TEA:SF-PDI2 (OPV)
PIPCP:PCBM (OPV)
PBDTTPD:PCBM (OPV)
E_G^{PV} 1 eV
2 eV
GaInP
$MAPbI_3$
GaAs
CdTe
InP
c-Si
CIGS
a-Si
CZTS
CZTSS
kT
qV_{OC}^{Rad}(eV)
Urbach Energy (meV)

(d)

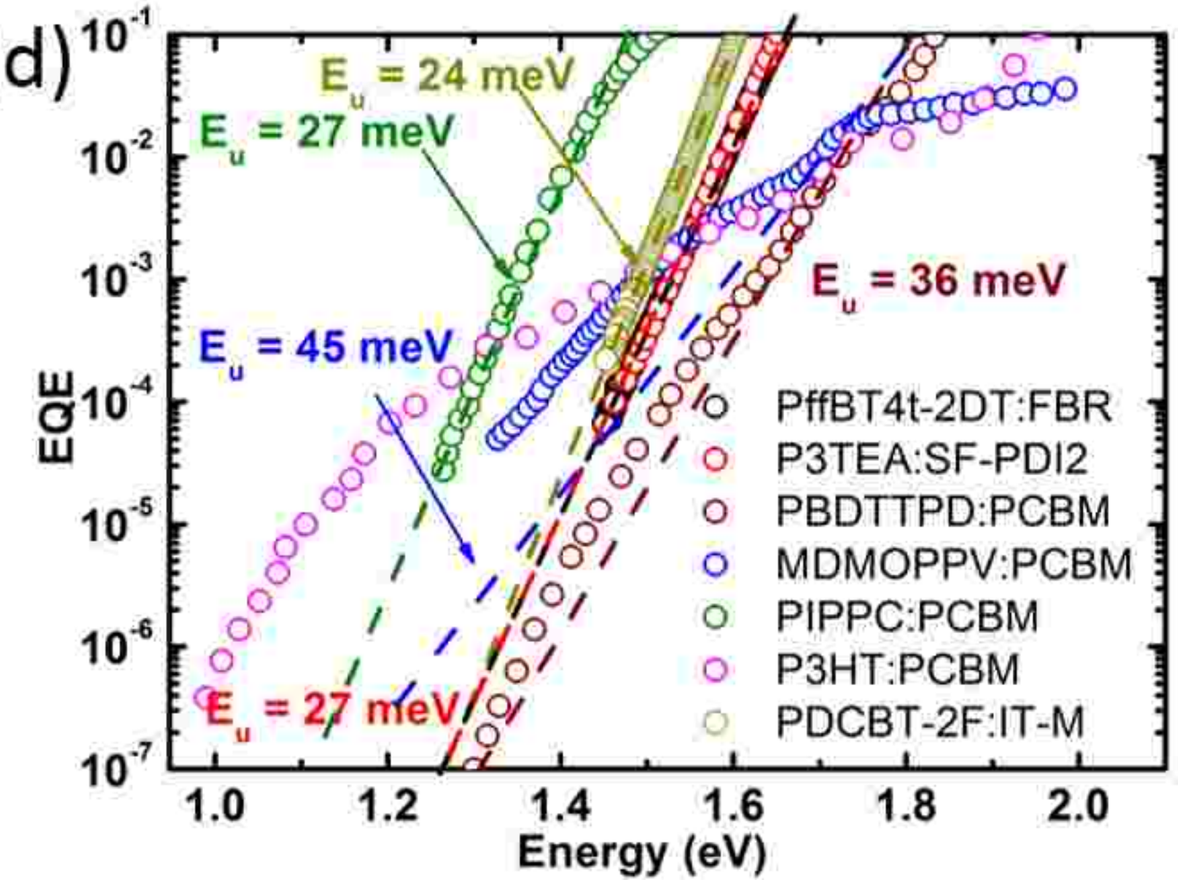
E_u = 24 meV
E_u = 27 meV
E_u = 36 meV
E_u = 45 meV
E_u = 27 meV
PffBT4t-2DT:FBR
P3TEA:SF-PDI2
PBDTTPD:PCBM
MDMOPPV:PCBM
PIPPC:PCBM
P3HT:PCBM
PDCBT-2F:IT-M
EQE
Energy (eV)

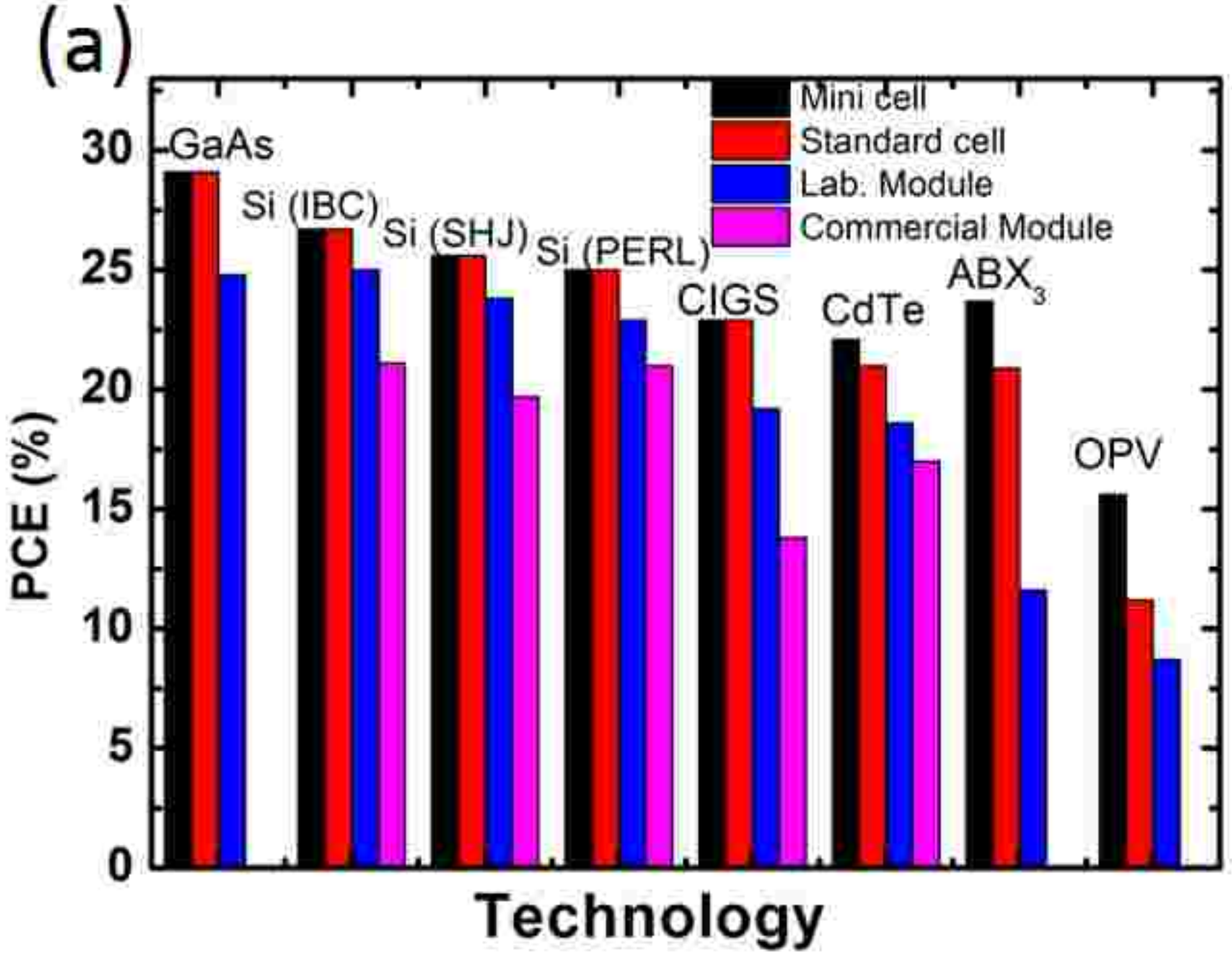
(a)
Mini cell
Standard cell
Lab. Module
Commercial Module
GaAs
Si (IBC)
Si (SHJ)
Si (PERL)
CIGS
CdTe
ABX3
OPV
PCE (%)
Technology

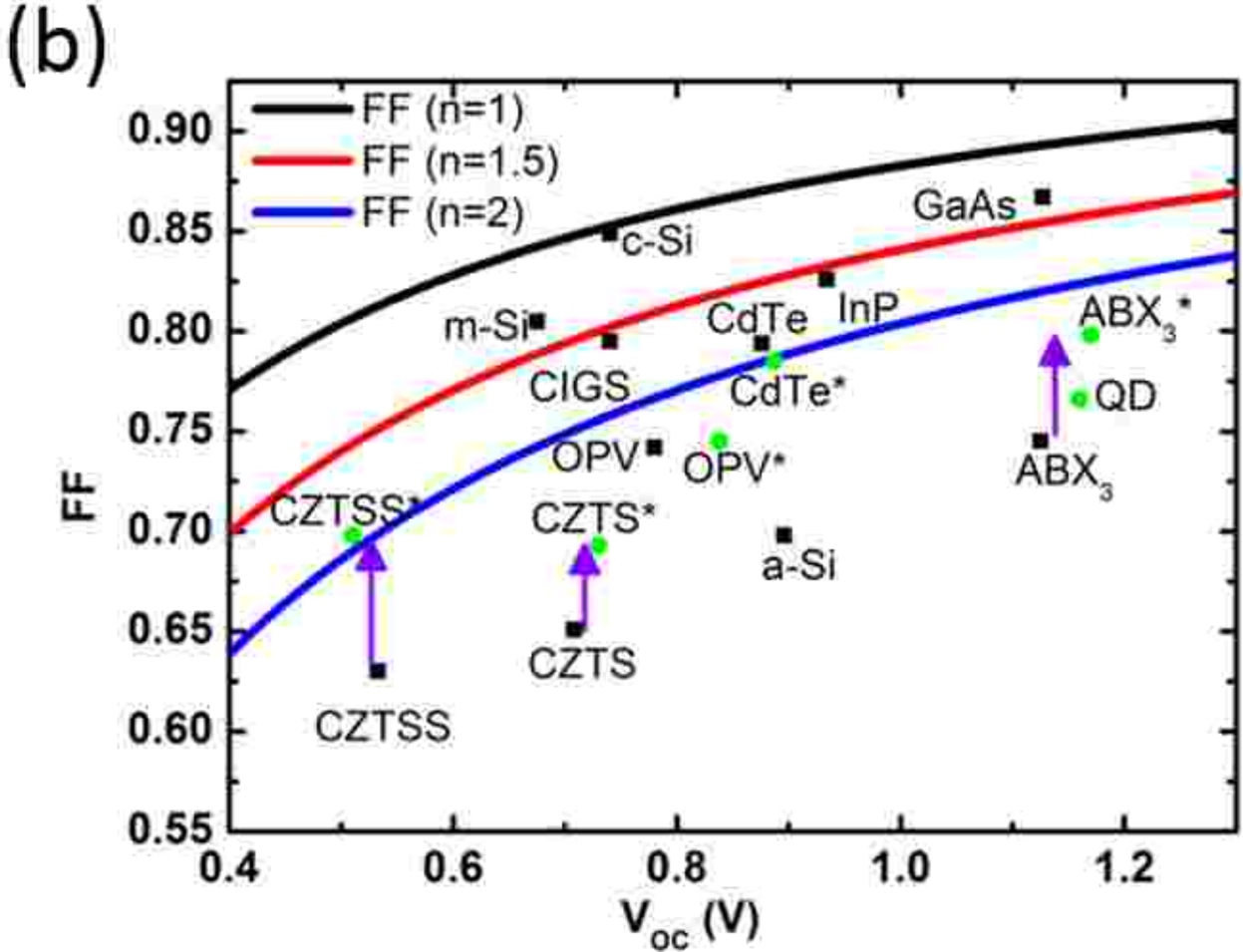
(b)
FF (n=1)
FF (n=1.5)
FF (n=2)
c-Si
GaAs
m-Si
CIGS
CdTe
InP
ABX3*
QD
CdTe*
OPV
OPV*
ABX3
CZTSS*
CZTS*
a-Si
CZTS
CZTSS
FF
Voc (V)